Reviewed Preprint
v1 • May 5, 2026
Not revised

For correspondence:
hirotay-gyn@h.u-tokyo.ac.jp

* These authors contributed equally.

Conflict-of-interest statement: The authors declare no conflict of interest.

Competing interests: No competing interests declared

Funding: See page 22

Reviewing editor: Wei Yan, Washington State University, United States



# A stress-responsive morphogenetic program of the uterine epithelium safeguards the establishment of early pregnancy

**Chihiro Ishizawa[1,*], Shizu Aikawa[1,*], Yamato Fukui[1], Xueting He[1], Ryoko Shimizu-Hirota[2], Daiki Hiratsuka[1], Mitsunori Matsuo[1], Takehiro Hiraoka[1], Yasushi Hirota[1]**

[1]Department of Obstetrics and Gynecology, Graduate School of Medicine, The University of Tokyo, Tokyo, Japan •
[2]Department of Internal Medicine, Center for Preventive Medicine, Keio University School of Medicine, Tokyo, Japan

## eLife Assessment

This **valuable** study reports the architectural reorganization of the uterine luminal epithelium during the implantation period. The data presented are **solid**, although improvements are needed. This work is of interest to reproductive biologists and physicians practicing reproductive medicine.

https://doi.org/10.7554/eLife.110844.1.sa2

## Abstract

Successful embryo implantation requires coordinated interactions between the endometrial epithelium, stroma, and the embryo, yet underlying mechanisms have not been fully understood. Using three-dimensional histological reconstruction combined with single-cell and spatial transcriptomics, we identify a previously unrecognized phase of luminal architectural reorganization preceding embryo attachment. Within a narrow peri-implantation window, the luminal epithelium rapidly remodels from a highly folded structure into a flattened, organized architecture that provides a scaffold for embryo positioning. This morphogenetic transition is accompanied by activation of stress-responsive signaling across epithelial and stromal compartments. Functional analyses show that uterine-specific deletion of the stress-responsive MAP kinase p38α disrupts luminal remodeling, leading to persistent epithelial folding, failed embryo attachment, and infertility despite normal hormone levels and embryo development. Although combined progesterone and leukemia inhibitory factor supplementation rescues embryo attachment in p38α-deficient uteri, luminal disorganization, abnormal stromal responses, and impaired pregnancy progression persist. These findings identify a p38α-dependent, stress-responsive morphogenetic program that coordinates epithelial dynamics and epithelial–stromal communication to establish implantation-competent luminal architecture.

## Introduction

Infertility is a social concern that affects 17.5% of the adult population worldwide[1]. Some patients who undergo in vitro fertilization and embryo transfer (IVF_ET) repeatedly fail to become pregnant, even after ET using high-quality embryos (2). Embryo implantation, which is the starting point of pregnancy, can be divided into several processes, including blastocyst spacing, apposition, attachment to the uterine luminal epithelium, and invasion into the endometrial stroma[2, 3]. Establishing implantation requires an exquisite interaction between the endometrium and embryo; however, the detailed underlying mechanism remains unclear.

Based on the similarities in the influence of female sex hormones on the endometrium during pregnancy, rodents have been utilized as an in vivo model of human pregnancy. In mice, day 1 of pregnancy is defined by the observation of a vaginal plug. After coitus, high serum levels of estrogen ($E_2$) induce epithelial proliferation and $P_4$ production from the ovary increases on day 3. Embryos in the oviduct reach the uterus on day 4 in a $P_4$-dominant hormonal environment. In the uterus, proliferation-differentiation switching (PDS), indicating the inhibition of epithelial proliferation with induction of stromal proliferation the endometrium, is evident on day 4 under the continuous influence of $P_4$, resulting in the endometrium acquiring implantation potential[4, 5]. With this dynamic change, the morphology of the endometrial luminal epithelium reveals a slit-like narrowing, known as the formation of a slit-like luminal structure[4, 6, 7] (Fig. 1a). Late on the morning of day 4, blastocysts are activated by a small estrogen surge that occurs as the starting signal for implantation[2,8]. The blastocyst finally attaches to the luminal epithelium on day 4 midnight. The luminal epithelium initiates the formation of a uterine crypt after attachment and the embryo can be observed at the bottom of the crypt[9]. Stimulation from the embryo attachment seems to be transmitted from the endometrial epithelium to the stroma, where vascular permeability is increased (attachment reaction), and the surrounding stromal cells initiate differentiation into decidual cells (decidualization). By the evening of day 5, the endometrial luminal epithelium facing the attached blastocysts disappears, and trophoblast invasion is initiated.

In recent studies, our group and others have demonstrated that a series of luminal changes, that is PDS, formation of a slit-like luminal structure, and crypt formation, are crucial for embryo implantation[4, 5, 6, 7, 9, 10, 11]. For PDS and formation of the slit-like luminal structure, the P - progesterone receptor (PGR) pathway is involved[4, 5, 6]. We previously reported that mice with epithelial deletion of Pgr ($Pgr^{fl/fl};Ltf^{Cre/+}$ mice; *Pgr* eKO) showed sustained epithelial cell differentiation, resulting in defective uterine receptivity[6]. As for embryo attachment and subsequent crypt formation, the Lif-Stat3 pathway is crucial, in addition to $P_4$-Pgr signaling. Leukemia inhibitory factor (Lif) activates uterine Lif receptors (Lifrs) to evoke Stat3-mediated gene transcription, thus initiating the formation of implantation chambers (crypts)[9, 11, 12, 13, 14]. We have also reported that uterine-specific retinoblastoma knockout mice (*Rb* uKO) and enhancer zeste homolog 2 knockout mice (*Ezh2* uKO) show impaired PDS because of cell cycle abnormalities in the endometrium[15, 16]. Notably, in these uKO models, although epithelial proliferation was continuously observed even on day 4, embryo attachment occurred but subsequent embryo invasion was flawed. These differential phenotypes of uterine-specific gene deletions suggest that essential mechanisms other than PDS are involved in $P_4$- and Lif-induced embryo attachment and subsequent pregnancy maintenance.

Accumulating evidence has demonstrated that PDS, slit-like formation, and crypt formation are important changes in the luminal epithelium for embryo attachment. However, how the overall changes in the luminal epithelia are dynamically regulated during the short period of embryo implantation remains unclear. It appears that PDS, slit formation, and crypt shaping occur sequentially; however, how each step influences the others remains uncertain. In particular, crypt formation occurs only in the presence of embryos[10], indicating that epithelial changes require reciprocal interaction with embryos. To understand the molecular mechanism underlying these epithelial changes, we especially examined p38α, a MAP kinase activated by phosphorylation in response to various environmental stresses and inflammatory cytokines, which regulates fundamental cellular processes such as proliferation, apoptosis, cell differentiation[17, 18, 19]. Notably, p38α plays an important role in development and tissue differentiation by modulating the localization of E-cadherin, which is expressed in tissue epithelial cells, thus altering epithelial morphology[20, 21]. Embryo implantation requires cell differentiation and death as well as glandular epithelial development and secretion, which may be influenced by p38α because it regulates various cell differentiation processes including mammary gland duct formation[22, 23, 24]. Recently, deletion of p38α was reported to result in complete pregnancy failure in mice[25], supporting our notion of a p38α-regulated mechanism shaping the endometrial epithelium during the peri-implantation period.

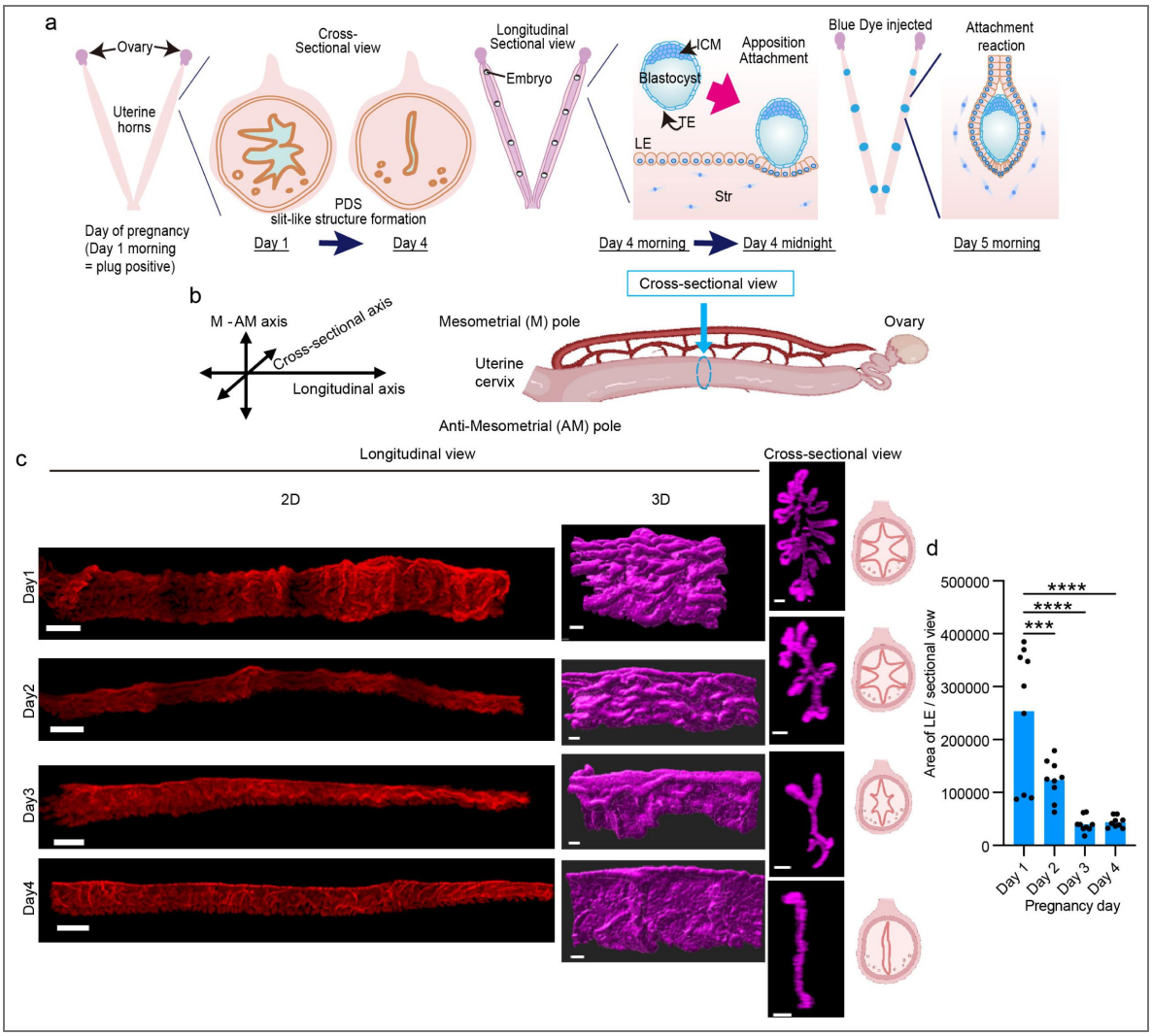


**Fig. 1. Three-dimensional observation of endometrial lumen morphology before embryo attachment.**

**a** A schematic diagram of embryo implantation. **b** Schematic of the longitudinal and cross-sectional views of the uterine horns. **c** Two-dimensional (2D) and Tridimensional (3D) views of the uterine epithelium stained for E-cadherin. The luminal epithelium was segmented and magenta colored using Imaris. Scale bar: 1 mm (left) and 200 μm (middle and right). Schematic diagrams of luminal shapes on each pregnancy day are shown in the right panel. **d** The area of the luminal epithelium per sectional view was quantified. n = 3 for each sample and n = 3 for each day of pregnancy; in total, n = 9 sections were quantified. Data are presented as means ± SEM, ***$P < 0.001$, ****$P < 0.0001$ by one-way ANOVA followed by Bonferroni's post-hoc test.

In this study, we first investigated the spatiotemporal changes of luminal shapes in 3D spanning the period from just after the coitus to the peri-attachment stage using a time course analysis. Our analyses revealed that the surface of the endometrial lumen not only became flattened but also showed creases, resulting in the even zoning of embryos before attachment. The embryos were then attached to the flattened area and crypts were formed. This epithelial shaping was impaired in the mice with uterine-specific knockout (uKO) of p38α, giving rise to failed embryo attachment. While treatment with $P_4$ and Lif restored embryo attachment in p38α uKO mice, embryo invasion and subsequent pregnancy maintenance remained disturbed because of abnormal epithelial shaping, which was not rescued. In summary, we discovered that dynamic morphological changes in the endometrial lumen prior to implantation may influence the process of pregnancy establishment and maintenance, which is regulated by previously unknown mechanisms independent of $P_4$-Pgr and Lif-Stat3.

# Results

## The morphology of the endometrial luminal surface dynamically changes before embryo attachment

To identify the spatiotemporal changes in the luminal epithelium prior to embryo attachment, we adopted 3D visualization, which recently revealed the detailed topography of the endometrial epithelium and the mechanism of embryo implantation[10]. Blood vessels enter the uterus from the mesometrium, situating the uterus along the mesometrial–anti-mesometrial (M–AM) axis. Once blastocysts attach to the surrounding luminal cells, an implantation chamber (crypt) is formed by luminal epithelial (LE) evaginations toward the AM pole[10, 26, 27] (Fig. 1a, b). Although the morphological changes in the endometrial lumen after embryo attachment have been reported[10, 28], little is known regarding the luminal morphology prior to attachment. How the epithelial dynamics prior to embryo attachment influence subsequent pregnancy processes also remains unclear.

Therefore, we analyzed the luminal morphology in wild-type mice on the mornings of days 1–4 of pregnancy. On day 1, the endometrial lumen extended in a disorderly manner against the M-AM plane. During days 2–4, the lumen became flattened with some folding in the M-AM axis that remained even (Fig. 1c). A cross-sectional view of the tissues revealed that the lumen became more slit-like with epithelial mass decreasing daily prior to embryo attachment (Fig. 1c, d), which was consistent with the results of luminal changes previously depicted using conventional histology[4, 29].

Next, we investigated the relationship between luminal folding and blastocyst movement by observing day 4 endometria from the morning to midnight, when blastocysts arrived and attached to the uterine lumen, respectively. We observed the 3D morphology of the uterine lumen and positions of the blastocysts on day 4 morning (day 4 10:00), day 4 evening (day 4 16:00), day 4 evening (day 4 20:00), day 4 midnight (day 5 0:00), and day 5 morning (day 5 10:00). Once embryo attachment occurred, vascular permeability increased in the surrounding endometrium, which could be observed by the injection of blue dye into mice (blue dye reaction)[30]. The blue dye reactions were 0% (0/5) at 16:00 on day 4, 18.8% (3/16) at 20:00 on day 4, 66.7% (4/6) at 0:00 on day 5, and 100% (7/7) at 10:00 on day 5 (Fig. 2a-c). Embryo attachment was completed in more than half of the individuals at midnight on day 4; therefore, we defined the evaluation time immediately before embryo attachment as day 4 20:00. As previously described, the surface of the endometrial lumen was flattened at day 4 10:00. On Day 4, from 16:00 to 20:00, the flat lumen exhibited alternating shrunken and stretched areas. Shrunken areas with multiple folds were observed at regular intervals. No regularity in the position of the embryos was observed until day 4 16:00; however, at day 4 20:00, the embryos entered the shrunken areas and gradually moved to the stretched areas over the time course. At day 4 midnight, the embryos were attached to the AM pole of the lumen in the stretched areas, and crypts were then formed on day 5 morning (day 5 10:00) (Fig. 2d). These results demonstrate that the uterus just prior to embryo attachment showed dynamic changes in luminal morphology once the embryos arrived.

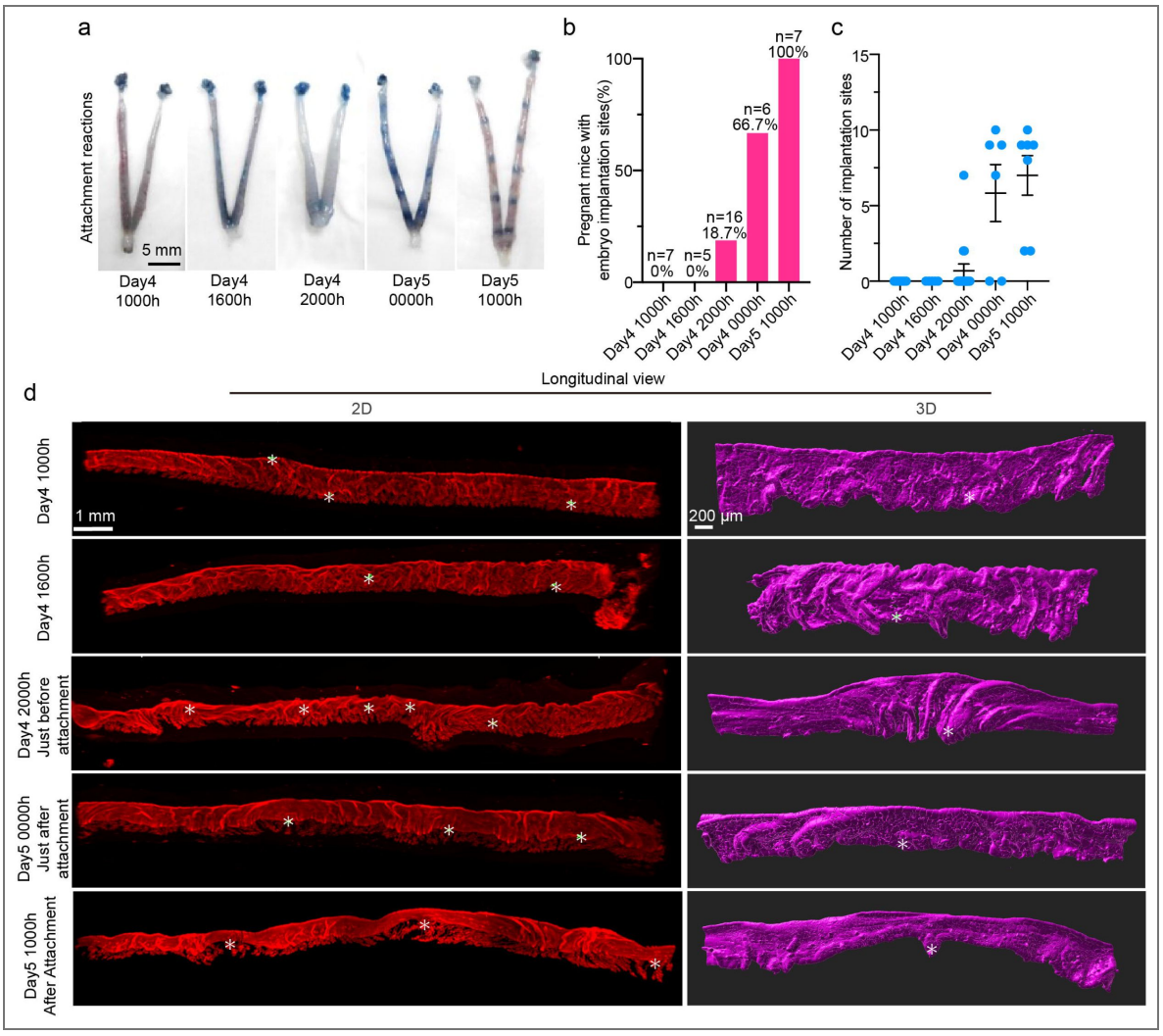


**Fig. 2. Dynamic morphological changes in the endometrial luminal epithelium occur on day 4 night, just before embryo attachment.**

**a** Representative photographs of pregnant uteri from day 4 morning to day 5 morning, which were injected with blue dye to depict embryo attachment sites. Scale bar: 1 cm. **b** Percentage of implantation-positive females in (**a**). The number of replicates and percentage of implantation-positive females are shown above each bar. **c** The number of implantation sites in (**a**) and (**b**). Data are represented as means ± SEM. **d** 2D and 3D longitudinal views of uterine epithelia stained for E-cadherin. In the right panels, the luminal epithelium is segmented and colored in magenta using Imaris. Scale bar: 1 mm (left) and 200 μm (right). Asterisks indicate the locations of embryos.

## Uterine p38α activation is crucial for luminal morphology and the subsequent embryo attachment

We then examined how luminal dynamics before attachment were regulated. We performed single-cell RNA-seq (scRNA-seq) analysis for days 4 and 5 uteri (Fig. 3). Uterine tissues contain multiple cell types, including epithelial, stromal, vascular endothelial (VE), and immune cells (Fig. 3a, Supplementary Fig. 1a, Table S1 and S2). Among them, luminal cell clusters (LE) can be divided into two types: conventional luminal cells (LE) which are highly observed on day 4, and activated LE (LE_activated), whose population increases on day 5 (Fig. 3a). To determine the characteristics of the LE_activated cells, we performed enrichment analyses using Enrichr[31] (Fig. 3b, Table S2). Transcription factor protein-protein interactions (PPIs) revealed enrichment of ATF2 and JUNB, which are related to stress signalling[32]. In agreement with this result, a pathway analysis using MSigDB HallMark also revealed TNFα-related and hypoxia signaling. Furthermore, gene ontology analysis using Metascape[33] identified pathways related to oxidative stress and cell motility (Fig. 3c, Table S2). We then investigated stromal cell types in the same manner (Fig. 3d, Supplementary Fig. 1b, and Table S3). These were clustered into five types: non-proliferative (Non-pro), proliferative (Pro), sub-epithelial (Sub-epi), sub-endothelial (Sub-endo), and attached (Attached). Because the day 5 stroma exclusively contained Attached cluster, we analyzed the enriched pathways in this cell type. Similar to LE_ activated, this cluster was enriched in stress-related transcriptional factors, signals and Gene Ontology (GO) terms (Fig. 3e, f, and Table S4).

As a possible regulator of day 5-specific LE and stromal cell types, we focused on p38α, a Map kinase protein. p38α is phosphorylated for activation in response to various kinds of cellular stimuli[18]. Notably, phosphorylated p38α (pp38α) translocates into nuclei to activate ATF2-JUN-induced transcription of cytokines, including TNFα[32]. Our immunostaining revealed that p38α was highly expressed and activated by phosphorylation in the pre-attachment luminal epithelia (Fig. 3g), indicating the role of p38α in the luminal epithelium before embryo attachment. After attachment, pp38α was expressed both in the endometrial epithelium and stroma, especially around the attached embryos on days 6 and 8.

To investigate the roles of uterine p38α, we established mice with uterine-specific deletion of p38α (p38α uKO) by crossing p38α-floxed mice with those carrying a Pgr-Cre driver. Efficient deletion and inactivation of p38α protein in p38α uKO was confirmed by immunostaining for p38α and pp38α (Fig. 4a). To examine the reproductive phenotypes of p38α uKO and littermate p38α-floxed females (p38α Ctrl), we mated them with fertile wild-type (WT) male mice. p38α uKO mice showed complete infertility (Fig. 4b). As we detected corresponding numbers of hatched blastocysts by flushing the uterine cavity with saline solution on day 4 morning in each genotype (Fig. 4c), uterine p38α did not influence embryo development before attachment. We then intravenously injected Chicago blue dye solution to examine the implantation sites on day 5 of pregnancy. However, p38α uKO uteri showed no attachment sites on day 5 of pregnancy, and blastocysts were recovered by saline flushing of the uterine cavities (Fig. 4d), which indicated flawed embryo attachment. On day 6 of pregnancy, the number of embryo attachment sites was significantly reduced in p38α uKO compared with those in the p38α uCtrl (Fig. 4e). Further, our 3D imaging on day 5 morning revealed failed crypt formation in p38α uKO, suggesting that p38α uKO mice show infertility because of embryo attachment failure (Fig. 4f).

Our observations indicating luminal activation of p38α in the pre-attachment period (Fig. 3g) as well as infertility with flawed embryo attachment in p38α uKO females (Fig. 4) motivated us to investigate the involvement of this molecule in luminal dynamics. We then compared the morphological changes in the lumen of p38α uCtrl and p38α uKO from days 1 to 4 using 3D imaging (Fig. 4g). Similar to the observation in the wild type mice, p38α uCtrl showed that the folding of the endometrial lumen in the M-AM axis gradually disappeared but some folding remained evenly. Accordingly, the endometrial lumen flattened as the pregnancy progressed from days 1 to 4. In contrast, in p38α uKO, folding in the both cross-sectional longitudinal axes remained

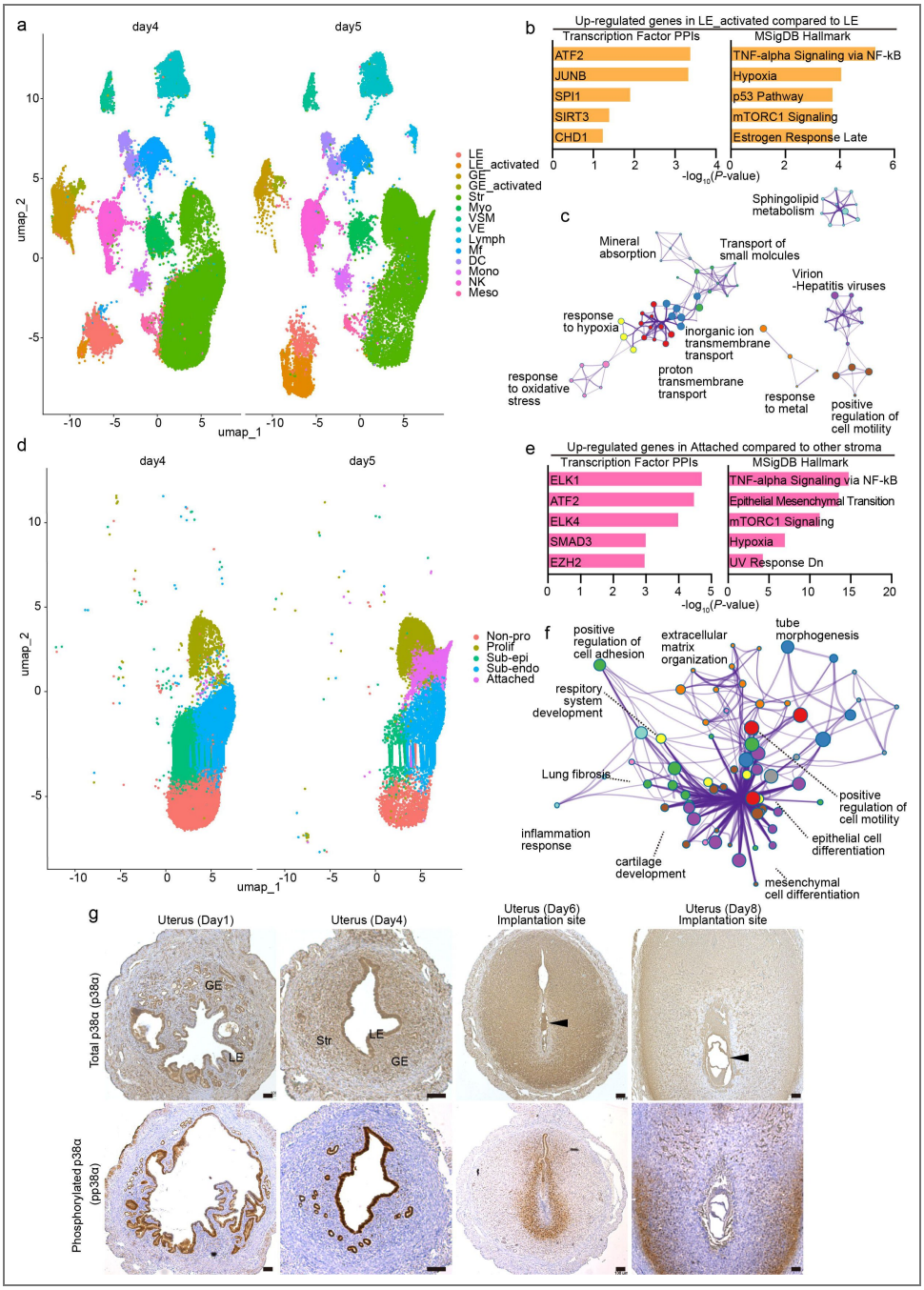


**Fig. 3. Stress-related signals are activated in the uteri during the peri-attachment phase.**

**a** UMAP of scRNA-seq cell types on days 4 and 5 of pregnancy. Dots indicate individual cells, and colors indicate different clusters. **b** Enrichment analyses for upstream transcription factors (left) and gene ontology (GO) (right) of highly expressed genes in the LE_activated vs. LE cells. **c** Network of GO terms related to the upregulated genes in the LE_activated cells compared with those in the LE cells. Each node represents an enriched term and is colored according to its cluster ID. **d** UMAP of different stromal cell types on days 4 and 5 of pregnancy. Dots indicate individual cells, and colors represent different clusters. **e** Enrichment analyses for upstream transcription factors (left) and gene ontology (GO) (right) of highly expressed genes in the Attached cluster compared with those in the other stromal clusters. **f** Network of GO terms related to the upregulated genes in the Activated cells compared with those in the other stromal clusters. Each node represents an enriched term and is colored according to its cluster ID. **g** Representative images of p38α (top) and phosphorylated p38α (pp38α; bottom) immunohistochemistry during days 1, 4, 6, and 8 of pregnancy. Scale bar: 100 μm. LE: luminal epithelia, GE: glandular epithelia, Str: Stroma, Em; embryo, Le; Luminal epithelium, St; Stroma. Arrowheads indicate embryos. At least three independent samples were evaluated for each day of pregnancy.

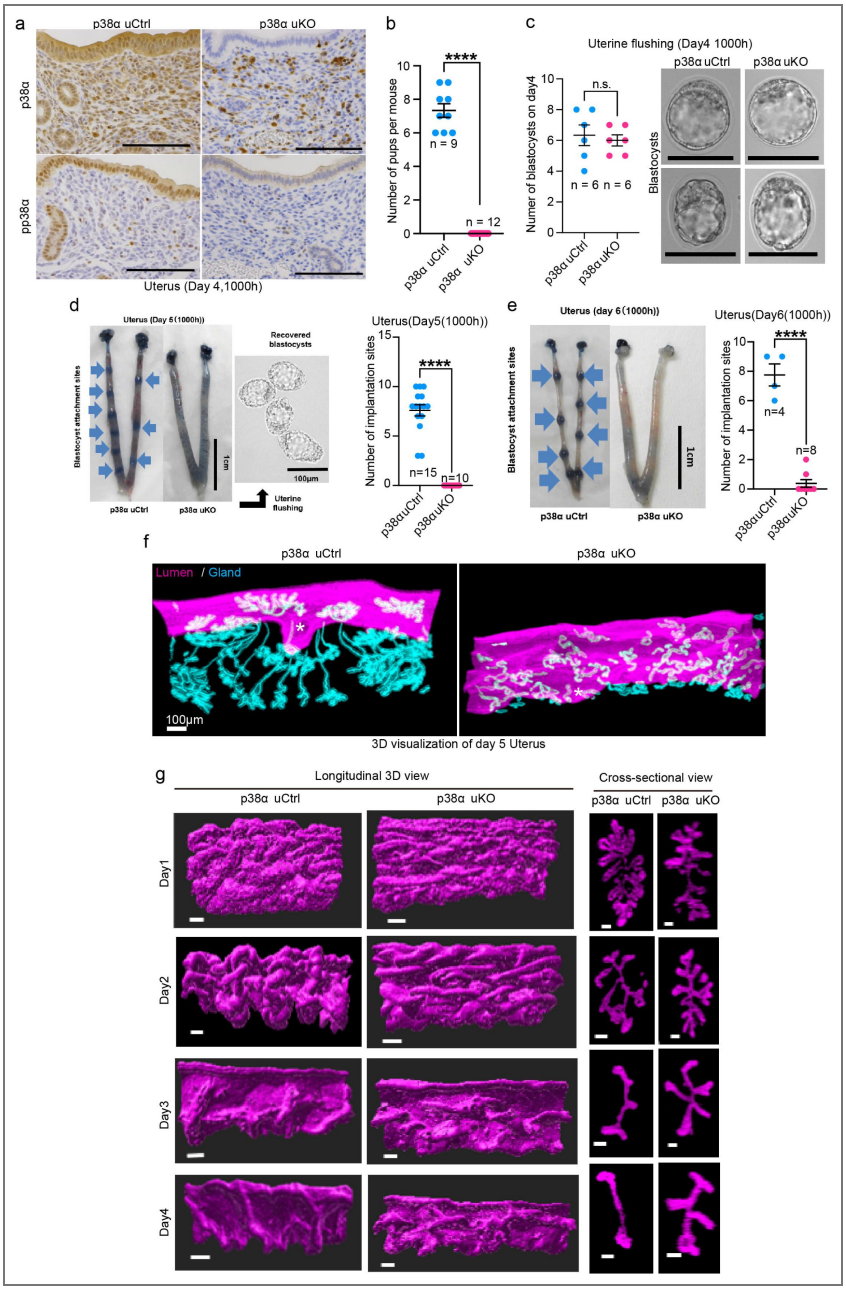


**Fig. 4. Morphological changes in the pre-attachment endometrial luminal epithelium are impaired in uterus-specific p38α KO mice.**

**a** Efficient p38α deletion was confirmed by immunostaining for p38α and phosphorylated p38α (pp38α) in the uteri on day 4 of pregnancy. Scale bar = 100 μm. **b** Average litter size for each genotype. The numbers of replicates are shown in the graphs. Data represent the mean ± SEM, and ****$P < 0.0001$ by Student's t-test. **c** Comparable numbers of flushed blastocysts (left) and their morphology (right). The graph shows the number of dams tested. Data represent the mean ± SEM, n.s.: not significant according to Student's t-test. **d** Representative photographs of the uteri from each genotype (left) and the average number of implantation sites on day 5 of pregnancy. Flushed embryos from p38α uKO are shown next to the uterine photographs. Scale bar = 1 mm (uteri) and 100 μm (embryos). The number of replicates is shown on the graph. Data represent the mean ± SEM, and ****$P < 0.0001$ by Student's t-test. **e** Representative photographs of the uteri from each genotype (left) and the average number of implantation sites on day 6 of pregnancy. Scale bar = 1 mm. The number of replicates is shown on the graph. Data represent the mean ± SEM, and ****$P < 0.0001$ by Student's t-test. **f** Representative images of day 5 pregnant uteri stained for E-Cadherin in 3D. The luminal and glandular epithelia were segmented and colored magenta and cyan, respectively. Scale bar = 100 μm. **g** Representative 3D views of luminal epithelia during days 1–4 of pregnancy, segmented based on epithelial staining for E-cadherin. Scale bar = 100 μm.

even on day 4, which appeared as serrated luminal shapes in the 2D view. Considering that embryo attachment failed in p38α uKO, the luminal changes in the pre-attachment phase could influence successful embryo attachment.

## Supplementation with $P_4$ and Lif, two major factors supporting embryo implantation, rescues the flawed embryo attachment, but not the subsequent pregnancy maintenance in p38α uKO

Our group and others have previously revealed that PDS, wherein epithelial cell proliferation is terminated before implantation, is an indicator of endometrial embryo receptivity[5]. P is an inducer of PDS as well as slit formation in the endometrial lumen[4, 6]. Immunostaining for Ki67, a cell proliferation marker, showed an increased number of proliferating cells in the luminal epithelium in p38α uKO on day 4 morning, suggesting that PDS was impaired in this milieu (Fig. 5a, b). This result motivated us to examine whether $P_4$ supplementation could rescue the phenotype of p38α uKO. We thus treated p38α uKO with $P_4$ in the preimplantation period and examined the resulting morphological changes in the endometrial lumen using 3D analysis. On days 3 and 4, $P_4$ treatment suppressed folding in both the cross-sectional and longitudinal axes, thus flattening the lumen (Fig. 5c-e). Further, PDS was also rescued by $P_4$ injection to p38α uKO (Fig. 5f, g). Notably, p38α uKO showed a normal hormone-producing capacity of the ovary, as serum estradiol-17β ($E_2$) and progesterone ($P_4$) levels were comparable (Supplementary Fig. 2a). We also confirmed that the expression of estrogen receptor (ERα) and progesterone receptor (PGR) in the uterus were not influenced by p38α deletion (Supplementary Fig. 2b). Although luminal morphology was improved by $P_4$ treatment, embryo attachment was still failed in the mutant (Fig. 5h), suggesting that some other factor is required for p38α-dependent embryo attachment.

Besides the $P_4$-PGR pathway, leukemia inhibitory factor (Lif) is a critical factor for embryo attachment[9, 11, 34]. Lif is an interleukin-6 family member secreted by the endometrial gland on the day 4 morning[34, 35, 36]. In situ hybridization showed significant decreases of Lif in the p38α uKO uterus on day 4 morning even after $P_4$ treatment (Fig. 6a). Further, activation of Stat3, a transcription factor downstream of Lif, was also downregulated as determined by immunostaining for phosphorylated Stat3 in p38α uKO uterus on day 4 morning (Fig. 6b). Based on these results, we examined whether activation of Lif-Stat3 can restore the flawed embryo attachment in p38α uKO.

These results prompted us to determine whether supplementation of Lif along with $P_4$ can ameliorate abnormal implantation in p38α uKO. Five groups were established: vehicle administration to p38α uCtrl and p38α uKO, $P_4$ alone to p38α uKO (at 10:00 on day 2–day 4), Lif alone to p38α uKO (at 9:00 and 18:00 on day 4), and both $P_4$ and Lif to p38α uKO (Fig. 6c). The number of embryo attachment sites in the single treatment of either $P_4$ or Lif did not differ compared with that in the vehicle group. In contrast, simultaneous supplementation with $P_4$ and Lif increased the number of embryo attachment sites in p38α uKO, which was comparable to that in the p38α uCtrl group as shown by the clear blue reactions on day 5 morning, indicating that both $P_4$ and Lif are required for p38α-dependent embryo attachment (Fig. 6d, e).

COX2 (Fig. 6f) and phosphorylated Stat3 (Supplementary Fig. 3), which are induced at embryo attachment sites[11], were found to be expressed in p38α uKO upon $P_4$ and Lif treatment, also supporting our notion. However, despite embryo attachment, $P_4$ and Lif treatment could not recover full term pregnancy with litters in p38α uKO (Fig. 6g). On day 8, although the number of implantation sites was comparable between the two groups, none of the implantation sites underwent normal embryogenesis and formed hematomas in p38α uKO treated with $P_4$ and Lif (Supplementary Fig. 4), indicating that pregnancy maintenance did not occur normally. Eventually, $P_4$ and rLif-treated p38α uKO females failed to give birth, accompanied by severe embryo resorption (Fig. 6g). This suggests that p38α is required for $P_4$- and Lif-induced embryo attachment as well as healthy pregnancy maintenance.

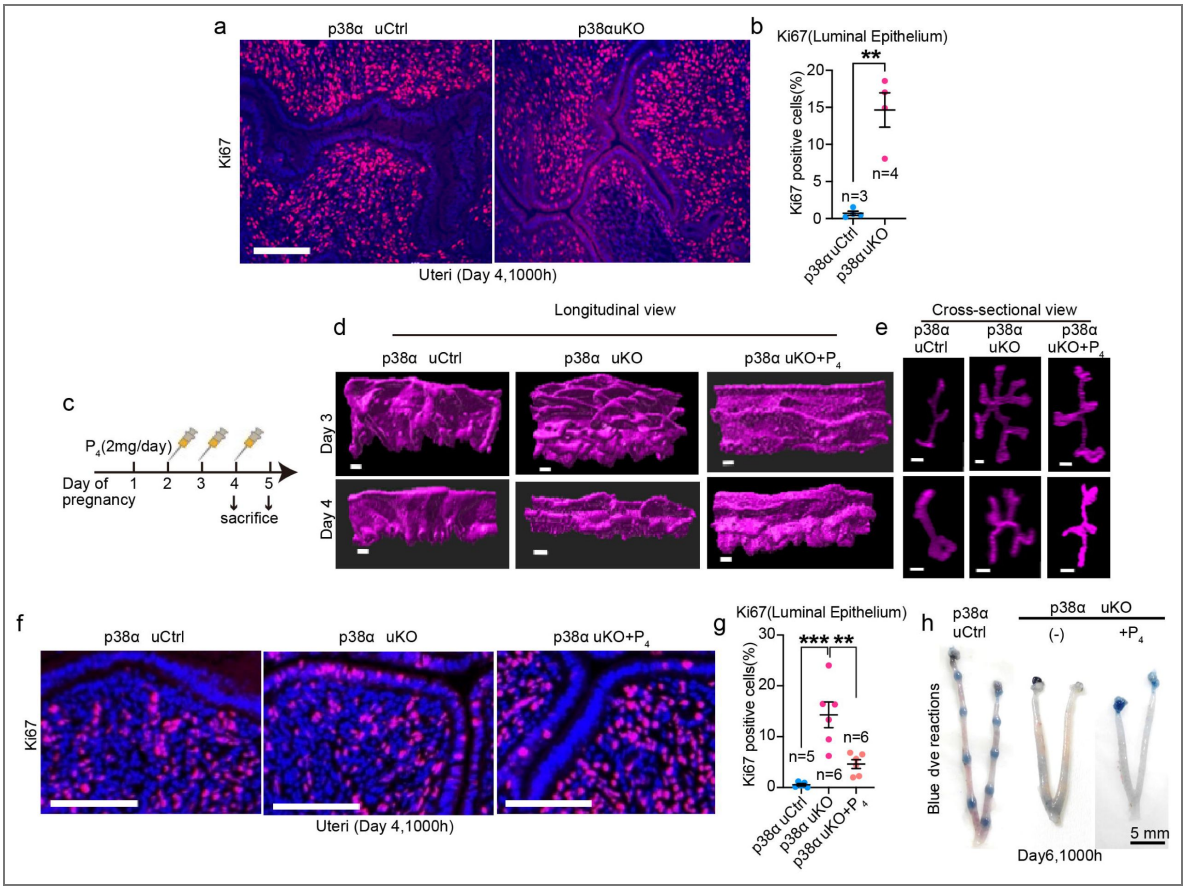


**Fig. 5. $P_4$ supplementation to p38α uKO mice partially rescues structural changes and proliferation-differentiation switching (PDS) in the endometrial luminal epithelium before embryo attachment.**

**a, b** Representative images of Ki67 immunofluorescence in the luminal epithelium of the uteri on day 4 morning. The percentages of Ki67-positive cells per total luminal cells are shown in (**b**). The number of replicates is shown on the graph. Data represent the mean ± SEM, $^{**}P < 0.01$ by Student's t-test. **c** The schedule of $P_4$ treatment to p38α uKO females during days 1 to 5 of pregnancy. **d** Representative 3D longitudinal views of luminal epithelia from the control and p38α uKO uteri with or without $P_4$ treatment, segmented from epithelial staining for E-cadherin. Scale bar = 100 μm. e Cross-sectional view of the luminal epithelia in (**d**). Scale bar = 100 μm. f, g Representative images of Ki67 immunofluorescence in the luminal epithelium on day 4 morning in the uteri from control and p38α uKO mice with or without $P_4$ treatment. The percentages of Ki67-positive cells per total luminal cells are shown in (**g**). The number of replicates is shown on the graph. Data represent the mean ± SEM, $^{**}P < 0.01$ and $^{***}P < 0.001$ by one-way ANOVA followed by Bonferroni's post-hoc test.

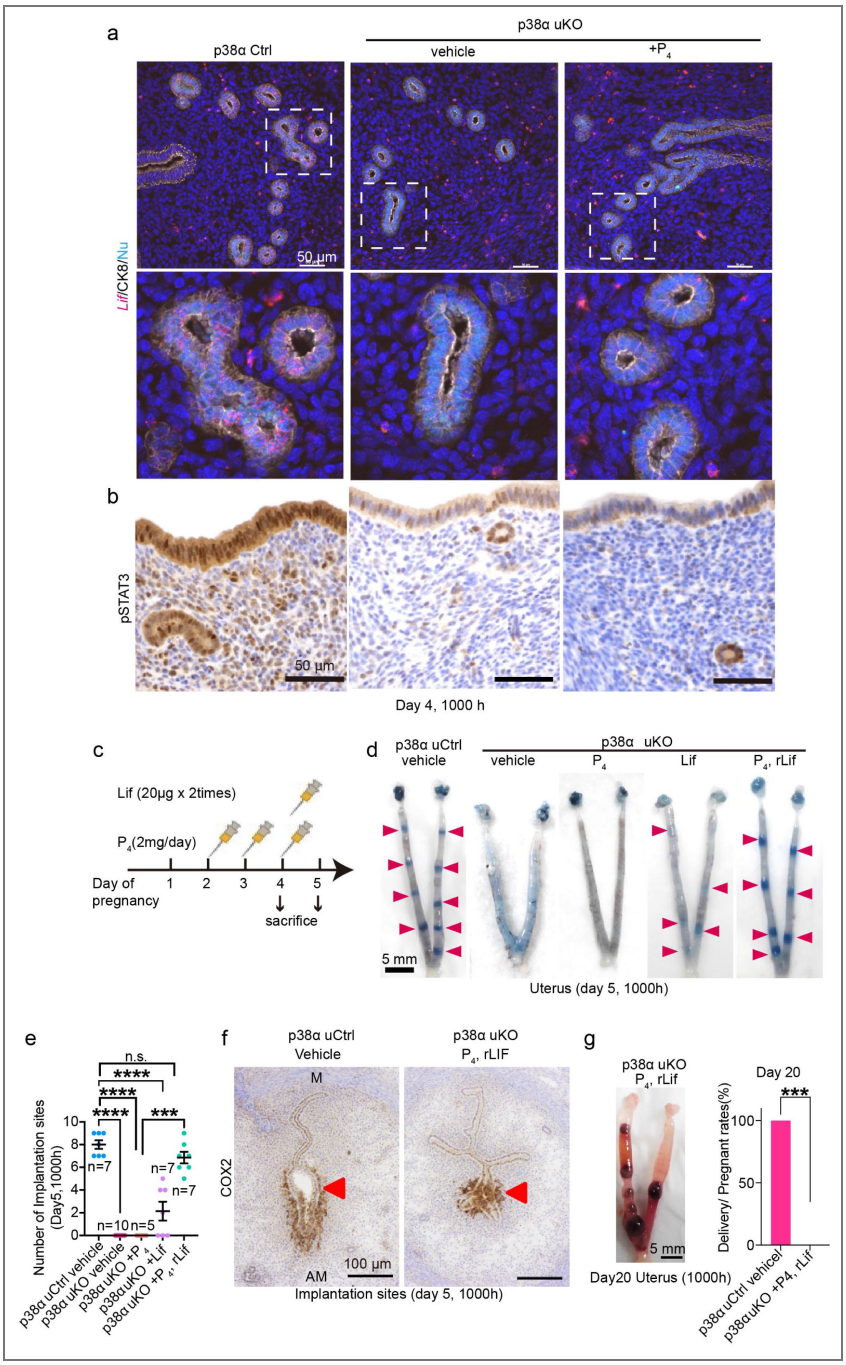


**Fig. 6. Impaired Lif-Stat3 pathway affects embryo attachment in p38α uKO mice.**

**a** Representative images of *Lif* in situ hybridization (top and middle) and phosphorylated Stat3 (pStat3) immunostaining (bottom) in day 4 uteri from control and p38α uKO mice with or without $P_4$ treatment. Epithelial cells immunostained for CK-8 are shown in the top and middle panels. The area indicated by a dashed line in the top panel is shown in the middle panel. Scale bar = 50 μm. **b** The schedule of $P_4$ and rLif treatment in p38α uKO female mice during days 1 to 5 of pregnancy. **c** Representative photographs of day 5 pregnant uteri from control and p38α uKO mice with or without $P_4$ and rLif treatment. Arrowheads indicate sites of embryo attachment. Scale bar = 5 mm. **d** The number of implantation sites in (**c**) was calculated. The number of replicates is shown on the graph. Data represent the mean ± SEM, ***$P < 0.001$, ****$P < 0.0001$ and n.s.: not significant by one-way ANOVA followed by Bonferroni's post-hoc test. f **e** Representative images of COX2 immunostaining on day 5 implantation sites from control and p38α uKO uteri treated with $P_4$ and rLif. Scale bar = 100 μm. M: mesometrial pole; AM: anti-mesometrial pole. Arrowheads indicate embryos. **f** A representative image of day 20 pregnant uteri from p38α uKO mice treated with $P_4$ and rLif. The percentage of deliveries per total number of pregnant females is shown on the right graph. The number of replicates is shown on the graph. Data represent the mean ± SEM, ***$P < 0.001$ by Student's t-test.

## p38α plays an important role in establishing the luminal epithelial morphology for embryo attachment, and changes by day 4 morning are an important scaffold for embryo attachment site formation

Flawed pregnancy maintenance in the mutant even after treatment led us to examine how pregnancy events after the embryo attachment were disturbed in p38α-deleted uteri. We thus investigated the luminal morphologies on days 5 and 6 when embryo attachment and invasion were evident (Fig. 7a). We found that folding was evident in the longitudinal axis in p38α uKO regardless of any treatment.

Simultaneous treatment with $P_4$ and Lif created a crypt on day 6, but still longitudinal folding was observed around the crypt. Further, crypt formation was poorly initiated on day 5 morning in $P_4$ and Lif-treated p38α uKO showing an obvious longitudinal folding. Considering that this folding should be eliminated by day 4 night in normal pregnancy (Fig. 2), we investigated the luminal morphology at day 4 20:00, just before embryo attachment (Fig. 7b). Similar to the preparatory phase of embryo attachment on day 4 morning (10:00 am), the surface of the stretched lumen, i.e., the site of embryo attachment, was flat in p38α uCtrl. In contrast, p38α uKO and p38α uKO+Lif ($P_4$ non-treated group) showed remarkable persistence of luminal folding in the longitudinal axis with a poorly established stretched area. In p38α uKO+$P_4$ and p38α uKO+Lif+$P_4$ ($P_4$ treated group,) the flattening and stretching of the lumen was partially rescued but longitudinal folding remained (Fig. 7b, left). We also observed the luminal shapes in cross-sectional views to examine the relationship between the shape of the slit-like lumen and embryo location (Fig. 7b, right, c, and d). In the p38α uCtrl, the stretched luminal areas serving as embryo attachment sites, were flat and slit-like, predicting smooth guidance of the embryo to the AM pole (Fig. 7b, right). In contrast, regardless of the treatment, flattening of the lumen failed in the p38α uKO, accompanied by strayed positioning of embryos probably because of failure of M-AM axis formation. These abnormal morphologies of the luminal epithelia appeared as an increased epithelial mass (Fig. 7c) and increased epithelial branching in the uKO (Fig. 7d). Overall, these results suggest that p38α is responsible for morphological changes in the lumen before embryo attachment, which $P_4$, but not Lif, partially assists in. Considering that $P_4$ could not solely restore embryo attachment in p38α uKO, Lif seems to act as an inducer of attachment under the influence of $P_4$.

## p38α is an important signal transducer between luminal epithelia and stroma for embryo attachment

We then examined how p38α influences feto-maternal interactions to accomplish healthy embryo implantation and luminal dynamics. Notably, we found that epithelial-specific deletion of p38α did not critically alter female fertility (Supplementary Fig. S5), indicating that p38α regulates epithelial-stromal crosstalk. To obtain this information, we performed scRNA-seq in Ctrl uteri on day 4 2000 h (just before attachment) and 2400 h (at attachment), as well as in uKO mice with or without $P_4$ + rLif treatment on day 4 2400 h (Fig. 8a, Table S5). Similar to Fig. 3a, we found multiple cell types in the uteri, including epithelial, stromal, myometrial, and immune cells. Among these, we focused on stromal cells as their population increased during the embryo attachment process in the uCtrl (Fig. 8a). The stromal cells were further clustered into non-proliferative (Non-prolif), proliferative (Pro), decidualizing (Dec), sub-epithelial (Sub-epi), sub-endothelial (Sub-endo), and uKO-specific clusters (Fig. 8b, Table S6). The uKO-specific cluster was highly enriched in uKO uteri. We then traced stromal differentiation using pseudo-time analysis (Fig. 8c and d). Intriguingly, the uKO-specific cluster was poorly differentiated compared with other stromal cell types, except for the Non-prolif cluster (Fig. 8d). We then examined the signal transduction between the epithelial (LE and GE) and stromal clusters, focusing on secretory molecules that can bridge the epithelial and stromal compartments (Fig. 8e). In uCtrl, non-canonical Wnt (ncWnt) from the LE and stroma and IGF from the stroma affected the decidualizing and luminal cells, which were enhanced upon embryo attachment (Fig.

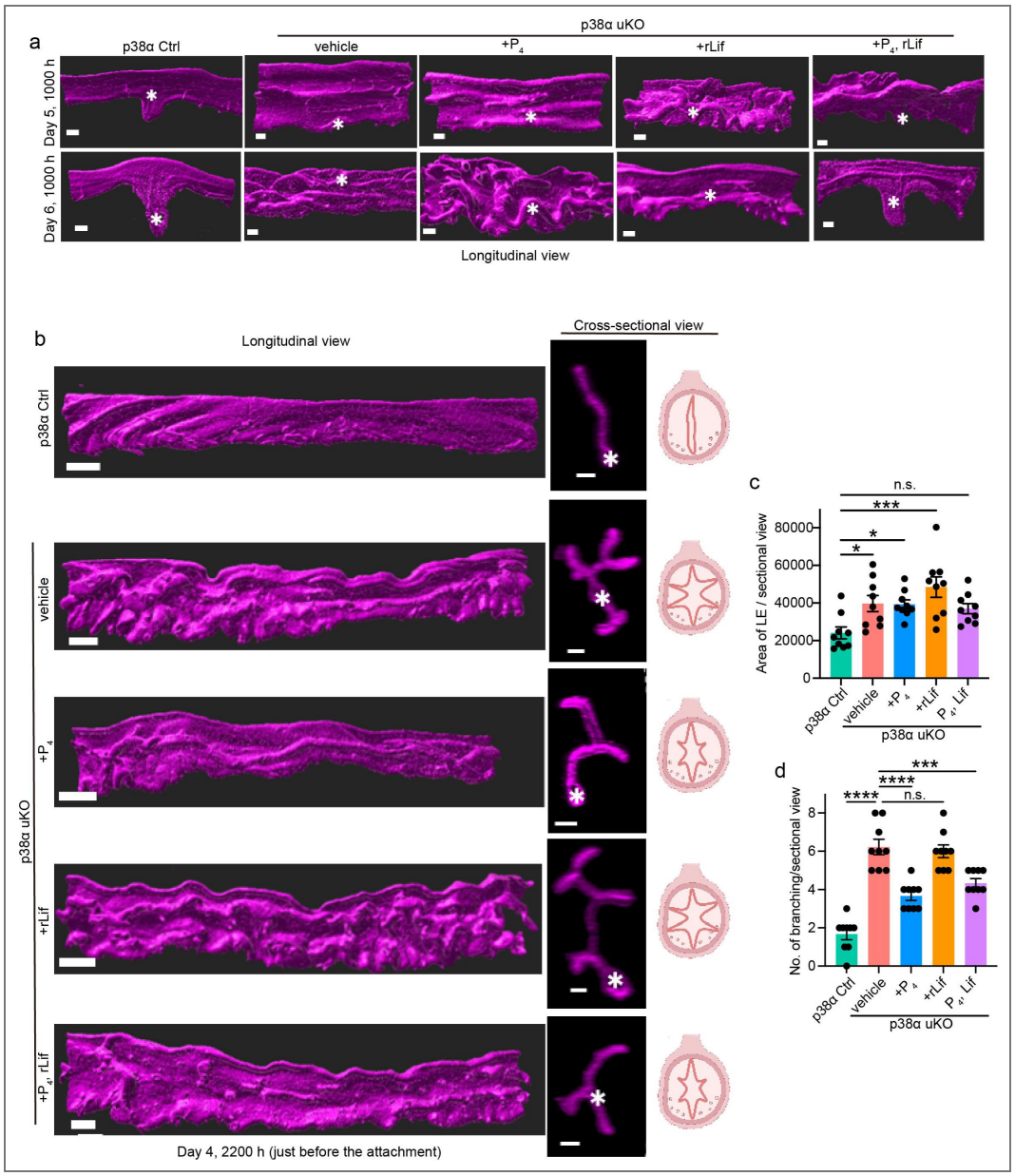


**Fig. 7. Embryo attachment in p38α uKO mice is rescued by supplementation with $P_4$ and Lif, but luminal positioning remains inappropriate.**

**a** Representative 3D views of the luminal epithelia collected from each genotype on days 5 and 6 of pregnancy. Scale bar = 100 μm, asterisks indicate embryos. b Representative 3D views of luminal epithelia on day 4 midnight, immediately before embryo attachment, collected from each genotype. Scale bar = 100 μm, asterisks indicate embryos. The graphs in the right panels show the luminal shapes for each genotype and condition. c Average area per sectional view calculated from the images shown in (b). Data represent the mean ± SEM, and *P*-values were determined by one-way ANOVA followed by Bonferroni's post hoc test. d Average number of luminal branches per sectional view calculated from the images shown in (b). Data represent the mean ± SEM, and **P* < 0.05, ****P* < 0.001, *****P* < 0.0001, n.s.: not significant by one-way ANOVA followed by Bonferroni's post-hoc test.

8e, upper). In contrast, in p38α-deficient uteri, only epithelial cells strongly sent and received signals (Fig. 8e, lower left), which remained even with $P_4$ and rLif treatment (Fig. 8e, lower right). These results demonstrate flawed epithelial-stromal communication in the p38α uKO milieu.

Among ncWNTs, Wnt5a plays a critical role in early pregnancy[27, 28]. Wnt5a activates receptor tyrosine kinases Ror1 and Ror2 in the uterus Both overexpression and deletion of Wnt5a compromises pregnancy outcomes owing to sustained apicobasal polarity in the luminal epithelia[27]. Similar to Wnt5a, Igf1 is also involved in epithelial depolarity and is highly expressed in day 4 uterine stroma, activating Igf1r and downstream Stat3 in the luminal epithelia[37]. Uterine-specific deletion of Igf1r results in flawed embryo attachment because of sustained epithelial polarity[37]. These contexts prompted us to examine these two molecules in the p38α uKO milieu. We first compared Wnt5a and Igf1 expression using scRNA-seq data and found significantly upregulated Wnt5a and downregulated Igf1 in both the luminal epithelia (LE) and decidualizing stroma (Dec) (Fig. 9a and b). In agreement with these results, we found stronger staining of epithelial markers, β-catenin and E-cadherin, in day 4 uKO uteri (Fig. 9c). We then asked whether embryo invasion was influenced by p38α deletion. Our group has previously shown that epithelial removal after the loss of epithelial polarity facilitates embryo invasion and the subsequent pregnancy processes[15, 38]. To assess embryo invasion, the implantation sites were stained for cytokeratin 8 (CK8), a marker of epithelial and trophoblastic cells. In p38α uCtrl, the endometrial luminal epithelium disappeared and trophoblasts invaded the uterine stroma on the morning of day 6, whereas the endometrial luminal epithelium around the embryo remained and embryo invasion was incomplete in p38α uKO even after treatment with $P_4$ and Lif (Fig. 9d).

We also examined the spatial transcriptome of the embryo attachment site on the morning of day 5 from Ctrl- and $P_4$ + rLif-treated uKO mice to observe epithelial-stromal interactions (Fig. 9e-h). Cross-sectional tissues of each implantation site were clustered into six types – LE, embryo attached stroma (Str_attached), proliferative stroma (Str_prolif), uKO-specific Str (Str_uKO_specific), GE, and myometria (Myo) (Fig. 9e, f, Table S7). Notably, uKO tissues solely contained Str_uKO_specific as the stromal cluster. To understand the characteristics of this cell type, pathway analyses were performed using Metascape. We found that the upregulated genes in Str_uKO_specific were enriched in pathways such as “regulation of inflammatory response,” “negative regulation of cell differentiation,” and “negative regulation of cell population proliferation” (Fig. 9g, Table S8)

Down-regulated genes were related to “Extracellular matrix organization,” “negative regulation of canonical Wnt signaling pathway,”, and “regulation of cellular response to growth factor stimuli” (Fig. 9h, Table S8), which are known to be associated with healthy pregnancy outcomes[36, 39]. These results indicate that embryo attachment to the uKO luminal epithelia induces inflammatory signals rather than physiological reactions in the stroma, compromising subsequent pregnancy maintenance. In summary, our data demonstrate the previously unappreciated role of uterine p38α as crucial for appropriate embryo attachment independently of the $P_4$ and Lif pathways.

# Discussion

Communication between embryos and endometria is crucial for the successful establishment of pregnancy[40]. In preparation for blastocyst attachment, the endometrium undergoes massive morphological changes, especially in the epithelial layers: (1) PDS before embryo attachment, (2) slit formation of the endometrial lumen before embryo attachment, and (3) crypt formation of the endometrial luminal epithelium after embryo attachment. In this study, we conducted 3D histological analysis as well as single cell and spatial transcriptome analyses to elucidate the details of dynamic morphological changes in the endometrial lumen. Two molecular pathways, the $P_4$-PGR and Lif-Stat3 pathways, have been considered important for embryo attachment so far. Further, we demonstrated a previously unappreciated role of p38α in addition to the above two major pathways (Fig. 10).

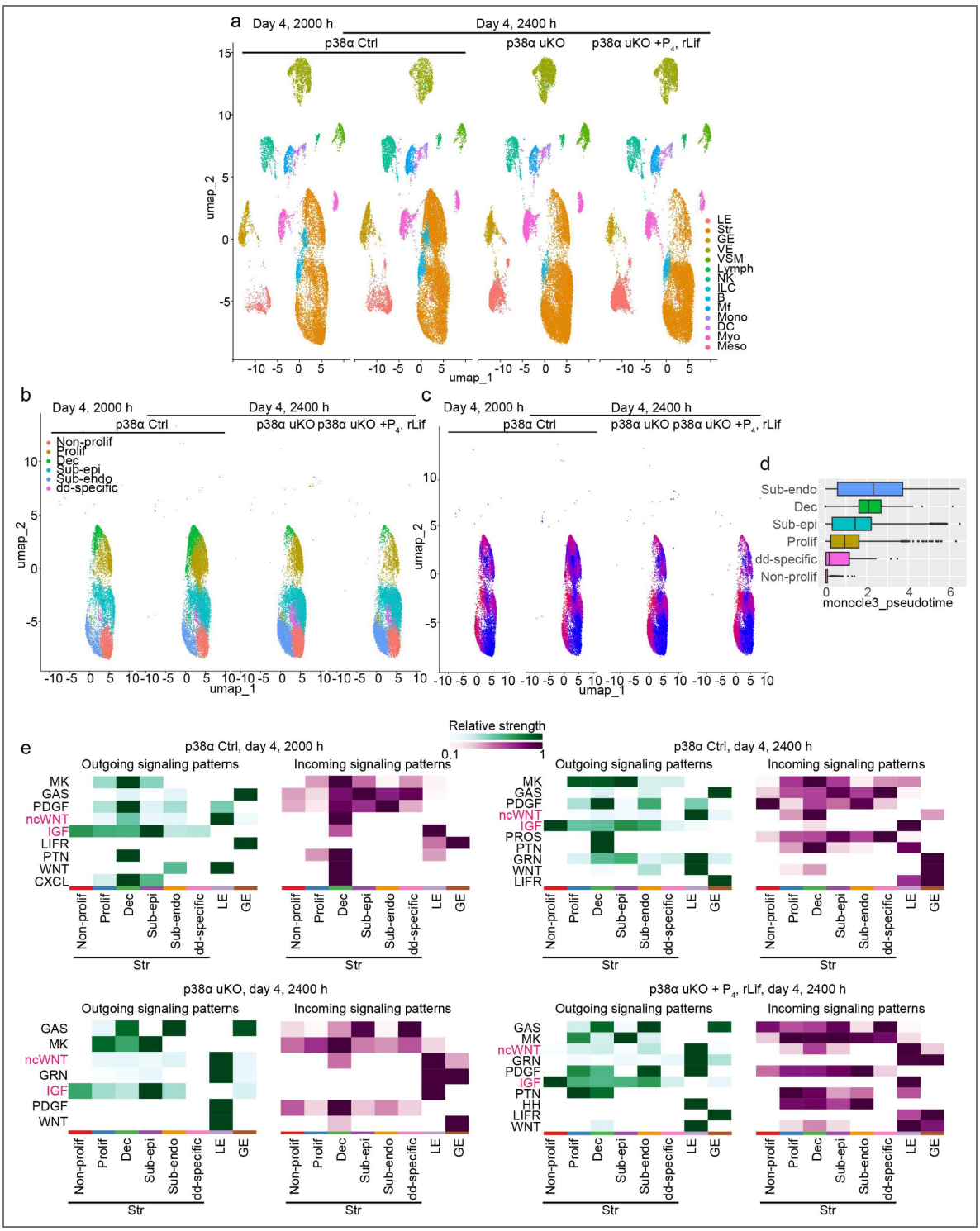


**Fig. 8. p38α plays an important role in stromal differentiation to ensure appropriate epithelial-stromal interactions before embryo attachment.**

**a** UMAP of scRNA-seq for various cell types from control uteri on day 4 evening and midnight, and from p38α uKO with or without $P_4$ and rLif treatment on day 4 midnight. Dots indicate individual cells, and colors indicate different clusters. **b** UMAP of scRNA-seq of stromal cell types from control uteri on day 4 evening and midnight, and from p38α uKO with or without $P_4$ and rLif treatment on day 4 midnight. Dots indicate individual cells, and colors indicate different clusters. **c** UMAP plots show the diffusion pseudotime of stromal cells. The colors of the spots indicate the pseudotime from early (blue) to late (dark red). **d** Boxplot showing the distribution of pseudo-time within different stromal cell clusters. Colors and labels indicate the cell types corresponding to those shown in (**b**). **e** Heatmap showing the outgoing (left) or incoming (right) communication strengths of key pathways between the major uterine endometrial cell types in each genotype and condition.

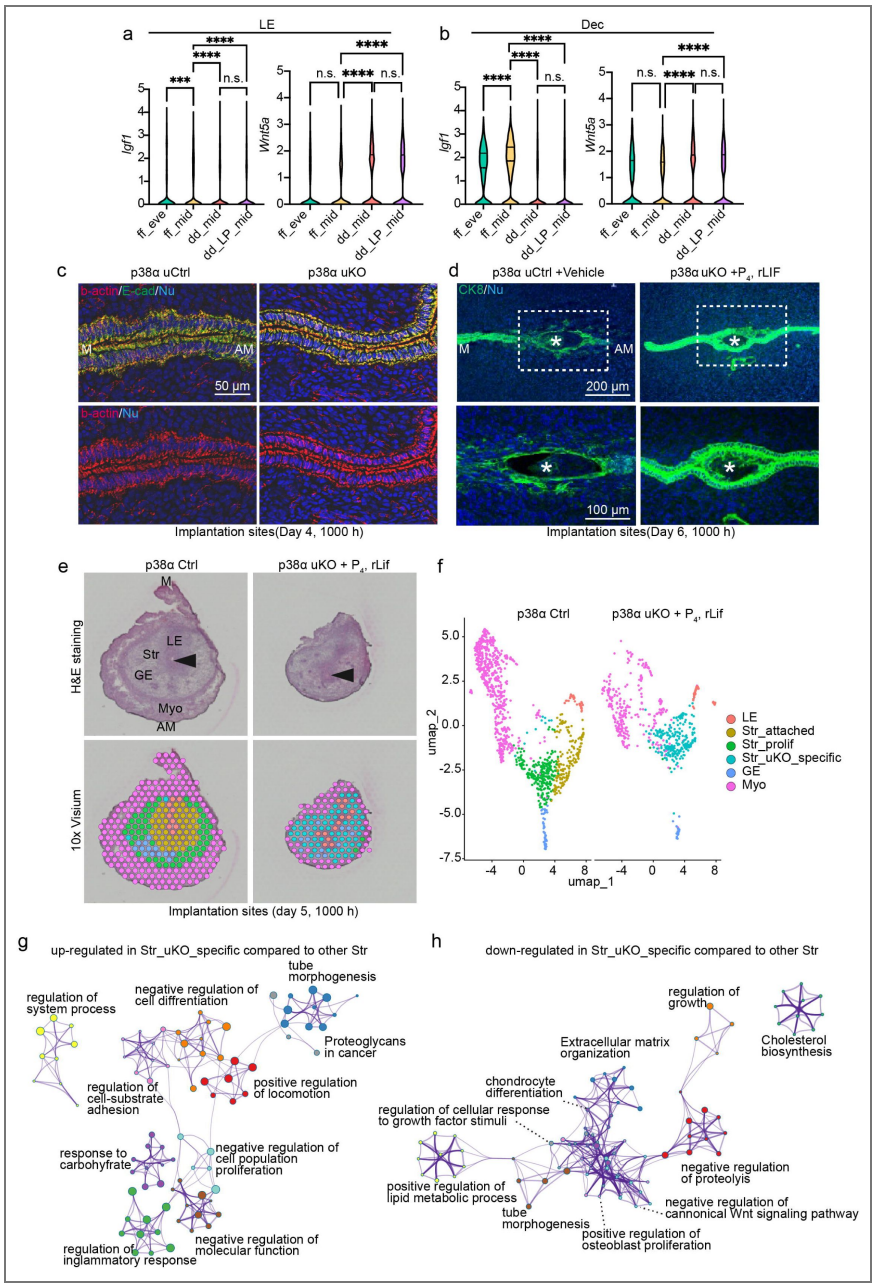


**Fig. 9. p38α uKO mice supplemented with $P_4$ and Lif show embryo invasion failure owing to sustained epithelial polarity.**

**a, b** Luminal epithelial (**a**) and stromal (**b**) expression of *Igf1* and *Wnt5a* determined using scRNA-seq in each genotype and condition. ***$P < 0.001$, ****$P < 0.0001$, ns: not significant by one-way ANOVA followed by Bonferroni's post-hoc test. **c** Representative images of immunostaining for β-actin (red) and E-cadherin (green) in day 4 uteri from each genotype. M: mesometrial pole, AM: anti-mesometrial pole. Scale bar = 50 μm. **d** Representative images of immunostaining for CK-8 (green) on day 6 implantation sites from the control and p38α uKO mice treated with $P_4$ and rLif. Areas demarcated by dashed lines in the top panels are shown in the bottom panels. M: mesometrial pole, AM: anti-mesometrial pole. Asterisks indicate embryos. Scale bar = 200 μm (top) and 100 μm (bottom). **e** H&E staining (upper) and visualization of the spatial transcriptome (lower) in day 5 implantation sites from the control and p38α uKO mice treated with $P_4$ and rLif. M: mesometrial pole; AM: anti-mesometrial pole, LE: luminal epithelia, GE: glandular epithelia, Str: stroma. Arrowheads indicate embryos. **f** UMAP analysis of the spatial transcriptome dataset colored according to cell type for day 5 implantation sites in control (left) and p38α uKO uteri treated with $P_4$ and rLif (right). Each dot color is mapped according to the spatial transcriptome visualized in the uterine sections, as shown in (**e**). **g, h** Network of GO terms related to the upregulated (**g**) or downregulated genes (**h**) in Str_uKO_specific compared to other stromal clusters. Each node represents an enriched term and is colored according to its cluster ID.

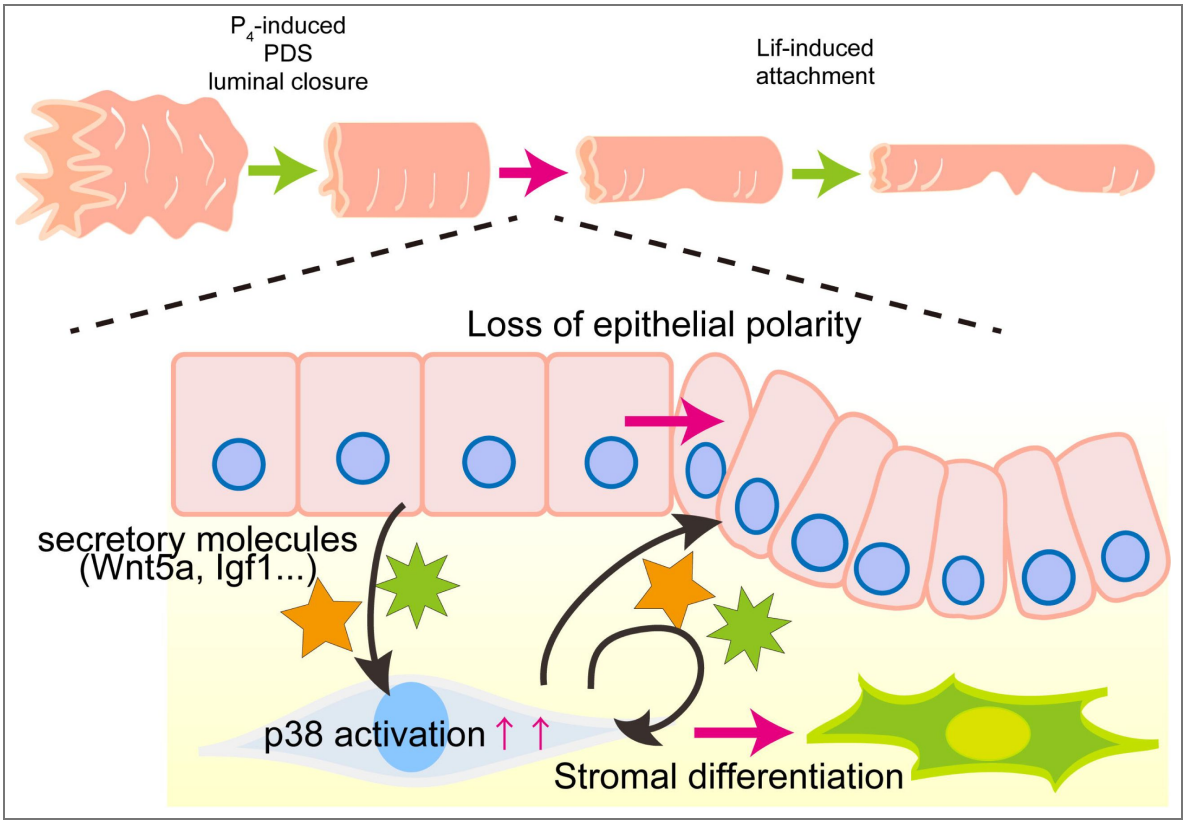


**Fig. 10. The role of uterine p38α in embryo attachment.**

p38α contributes to flattening of the endometrial luminal surface and induction of luminal narrowing prior to embryo attachment, through pathways activated by $P_4$. It is also suggested that uterine p38α induces glandular Lif, thus inducing embryo attachment. In addition to these pathways, p38α contributes to a decrease in epithelial polarity by activating epithelial-stromal interactions, thus resulting in successful embryo attachment and invasion.

The major finding of this study was that luminal shapes were altered throughout the uterine horns during early pregnancy. In particular, changes were evident from the morning of day 4 to midnight. This may explain the mechanism of embryo attachment as well as embryo spacing: a previous study demonstrated that embryo spacing occurs during day 4 noon to evening, which was compromised in mice with systemic KO of Lpar3, a lipid receptor expressed in the luminal epithelia[41]. Indeed, we observed that epithelial folding in the M-AM axis gathered evenly, corresponding to the position of the embryos from morning to evening on day 4, indicating that luminal layer movement contributes to embryo spacing in addition to myometrial, as previously reported[42]. This 3D imaging experiment had some limitations. Because the data were obtained from euthanized mice, following changes over time in the same individual was impossible, and the influence of phenotypic time differences among individuals could not be completely ruled out. To examine the epithelial morphology and phenotype over time in the same individual, experimental system using techniques such as live imaging in vivo needs to be established.

Considering the functional feature of p38α as a Map kinase, the outer- or inner-cellular stimuli evoking p38α-dependent epithelial shaping remain unclear. Map kinases can be activated downstream of various receptors, including tyrosine receptor kinases and G protein-coupled receptors[18]. One candidate is the Ror1/Ror2 tyrosine receptor kinase, which can be activated by Wnt5a[27]. Uterine-specific deletion of Wnt5a-Ror1/Ror2 axis resulted in defective embryo implantation because of abnormal luminal morphology, similar to our observation in p38α uKO. Similarly, deletion of Igf1-Igfr signaling causes poor embryo attachment, accompanied by abnormal luminal integrity[37]. These contexts may explain why Wnt5a and Igf1 were upregulated in p38α uKO uteri.

New insights into the morphological changes in the endometrial lumen may provide an innovative approach for treating embryo attachment failure, focusing on the endometrial lumen morphology. In humans, healthy implantation occurs at the fundus of the uterus[43], which is different from that in rodents with turbinal uterine structures. However, epithelial integrity is a common feature that regulates appropriate embryo implantation across species; for instance, after ovulation in humans, epithelial-mesenchymal transition with reduced epithelial polarity occurs during menstruation and implantation, thus influencing implantation outcomes[44, 45, 46]. A previous study using human endometrial epithelial cell lines demonstrated that deletion of p38α influenced the cellular transcriptome and metabolome, contributing to cancer cell-like characters[47], suggesting the role of p38α in maintaining luminal epithelial integrity in humans. In addition to specific molecular mechanisms, implantation failure may also be overcome from the mechanical aspect of tissue mobility for pathological conditions such as uterine myoma and uterine adenomyosis, wherein abnormal morphological changes in the endometrial lumen are presumed[48]. These findings are expected to have broad applications in diagnosing and treating human implantation failure, including the search for biomarkers of implantation ability and supplementation with relevant molecules. As reported previously, p38α also plays critical roles in mammary gland lumen formation[22]; therefore, the mechanism discovered in this study could be applicable in other epithelial systems as well.

# Methods

## Mice

WT (C57BL/6N, SLC), *p38*α-floxed (*Mapk14*-floxed; kindly provided by Dr. Kinya Otsu, University of Osaka)[19], *Pgr-Cre*[49], were used in this study. *Pgr-Cre* is expressed throughout the uterine layers[49]. Mice with p38α deletion in all uterine layers ($Mapk14^{flox/flox}$ $Pgr^{Cre/+}$; p38α uKO) were generated by crossing *Pgr-Cre* with *p38*α-floxed mice. Cre-negative littermates ($Mapk14^{flox/flox}$) served as controls. All mice used in this study were housed at the University of Tokyo Animal Care Facility, following the institutional guidelines for using laboratory animals.

## Evaluation of pregnancy outcomes

To examine the pregnancy outcomes, p38α-uKO, or p38α-floxed (control) female mice were mated with C57BL/6N fertile male mice, as reported in a previous study[15, 38, 50]. The day of vaginal plug detection was considered day 1 of pregnancy. Pregnant mice were euthanized by cervical dislocation on the designated day of pregnancy to evaluate pregnancy phenotypes and for sample collection. On days 2 and 3, both sides of the oviducts were flushed with saline to confirm the presence of 2-cell embryos on day 2 and 8-cell embryos or morula embryos on day 3. On day four, one uterine horn was flushed with saline to confirm the presence of blastocysts. Embryo attachment sites were observed as blue bands soon after intravenous injection of a 1% solution of Chicago blue dye (Sigma-Aldrich) in saline on days 5 and 6. When no embryo attachment sites were observed as of day 5, both uterine horns were cut and flushed with saline to collect the embryos.

To analyze implantation failure, pregnant mice were sacrificed on day 8 at 1000 h, and implantation sites were histologically assessed. If obvious hematopoietic cell infiltration was observed, implantation failure was diagnosed. Parturition events were monitored daily from days 19 to 22; all mice were dissected, and the abdominal cavity was observed for findings of miscarriage.

To evaluate the phenotype of embryo attachment in wild-type mice over time, we observed the uteri on day 4 morning (day 4 10:00), day 4 evening (day 4 16:00), day 4 night (day 4 20:00), day 4 midnight (day 5 0:00), and day 5 morning (day 5 10:00). For day 5 night, the observation time was defined as 18:00–22:00. In preliminary experiments, we confirmed that the phenotypes were equivalent, with no significant changes in the morphology of tissues collected during these 4 h. As described above, samples with visible embryo attachment sites were evaluated for their numbers, and those with no visible embryo attachment sites were evaluated as pregnant specimens by flushing the contralateral uterus with saline and observing the blastocysts. Daily subcutaneous injections of $P_4$ (2 mg/mouse/day) to p38α uKO mice were performed from day 2 of pregnancy or from the criterion day of pregnancy at 10:00 as previously described[15].

rLif injections were performed as previously reported[11]; female mice received rLif (20 μg/head, i.p.) at 9:00 and 18:00 on day 4 of pregnancy. The rLif expression vector was a kind gift from Prof. Eichi Hondo[13].

## Transmission electron microscopy (TEM)

TEM was performed on mouse uterine specimens collected on day 4 at 10:00 h. The fixation solution was 2% glutaraldehyde-2% paraformaldehyde dissolved in 0.1 M phosphate buffer (pH 7.4). The mice underwent the following perfusion procedures: deep anesthesia was administered, the mouse was fixed in place, and the abdomen to chest was incised; the diaphragm was quickly incised with tweezers and the heart was exposed; next, a 26G needle was inserted into left ventricle, and saline solution was injected; then, the saline was switched with the aforementioned fixative solution, which was injected to ensure fixative solution spreading to the tissues. Finally, the specimens were kept refrigerated in fixative solution. Specimen processing and imaging were performed at the Hanaichi Institute of Chemical Microscopy after embedding.

## RNA extraction and real time-quantitative PCR (RT-qPCR)

RNA was prepared from homogenized frozen tissues, as previously described[16]. qRT-PCR was performed using THUNDERBIRD SYBR qPCR Mix (TOYOBO). The housekeeping gene *Actb* was used for internal standardization of mRNA expression. Relative expression levels were determined using the ΔΔCt method[51]. The following primers were used.

| Gene | Strand | Sequence |
|---|---|---|
| Mouse *Actb* | Forward | TGTTACCAACTGGGACGACA |
| | Reverse | GGGGTGTTGAAGGTCTCAAA |
| Mouse *Lif* | Forward | GCTATGTGCGCCTAACATGA |
| | Reverse | AGTGGGGTTCAGGACCTTCT |
| | Reverse | CCTGATTAAACACAGCCCAGCA |
| *Mouse Cdh1* | Forward | TGATGTTGCTGTCCCCAAGT |
| | Reverse | CATCAACCGGCTTAATGGTG |

## H&E staining and immunostaining

H&E staining and immunostaining of uterine tissues were performed using paraffin-embedded sections (6 μm) or frozen sections (12 μm) as previously described[15]. For immunohistochemistry, the sections were incubated overnight with primary antibodies including p38 (8690, Cell Signaling Technology, 1:800), pp38 (4511, Cell Signaling Technology, 1:800), Esr1 (ab32063, Abcam, 1:200), Pgr (ab63605, Abcam, 1:100), pStat3 (ab76315, Abcam, 1:100), FOXA2 (8186, Cell Signaling Technology, 1:200), and COX2 (AA570-598, Cayman,1:200). For immunohistochemistry, signals were detected using a DAB substrate kit (#425011, Nichirei) after incubation with horseradish peroxidase-conjugated secondary antibodies (K4003, Dako). The images were captured using the Leica DM5000 B light microscope.

For immunofluorescence analysis of the paraffin sections, the sections were incubated overnight with primary antibodies, including CK8 (DSHB, 1:500), and signals were detected using Alexa Fluor 488-conjugated anti-rat immunoglobulin G (Thermo Fisher Scientific, A11006,1:500); nuclei were stained with 6-diamidino-2-phenylindole (DAPI) (Dojindo, 1:500). For immunofluorescence analysis of frozen sections, sections were incubated overnight with primary antibodies, including Ki67 (20701, Cell Signaling Technology, 1:200, Alexa Fluor® 555 Conjugate), Ecad (3199, Cell Signaling Technology,1:200, Alexa Fluor® 488 Conjugate), and β catenin (83539, Cell Signaling Technology, 1:200, Alexa Fluor® 555 Conjugate). Nuclei were detected using 6-diamidino-2-phenylindole DAPI (1:500). Images were captured using an AXR microscope (Nikon).

## Automated western blots with simple western (WES)

Proteins were extracted from cryopreserved and homogenized day 4 uterine tissues using RIPA buffer (Sigma) supplemented with a proteinase inhibitor cocktail (Sigma) and phosphatase inhibitor cocktail (Sigma).

Equal amounts of protein (2 μg/μl) were loaded into 12–230 kDa separation module kit and analyzed using the Protein Simple Wes® System (Protein Simple, San Jose, CA, USA) following the manufacturer's instructions. The antibodies used included Actin (C-11, sc-1615, Santa Cruz, 1:2000), Stat3 (4904, Cell Signaling Technology, 1:2000), and pStat3 (9145, Cell Signaling Technology, 1:2000). Anti-goat IgG and anti-rabbit IgG antibodies were used as secondary antibodies. Actin served as the loading control.

## 3D visualization of uterine endometrial luminal epithelium

3D visualization of the day 1–4 uteri or day 5 and 6 implantation sites was performed as previously reported[10]. To stain luminal and glandular epithelial cells, day 1–6 tissues were incubated with anti-E-cadherin antibodies (Cell Signaling Technology, 24E10, 1:500), followed by incubation with an anti-rabbit antibody conjugated with Alexa 555 (A21428, Thermo Fisher

Scientific, 1:500). 3D images were acquired using the LSM 880 (Zeiss) and AXR (Nikon) microscopes. The surface tool in Imaris (version 9.8; Oxford Instruments) was used to construct a 3D structure from the images.

## Measurement of serum $E_2$ and $P_4$ levels

Blood samples were collected from mice on the indicated day of pregnancy. Serum $P_4$ levels were measured as described previously[38], using a progesterone enzyme-linked immunosorbent assay (ELISA) kit (582601, Cayman). Serum $E_2$ levels were measured using an estradiol ELISA kit (501890, Cayman).

## Spatial transcriptomics

Spatial transcriptomes were analyzed using 10x Visium (10x Genomics) following the manufacturer's protocol. Day 6 uteri from control and Taz-uKO females were collected. Frozen sections (10 μm) were mounted on gene expression slides and sent to KOTAI Bio Inc. (Osaka, Japan) for processing. Following a 30-minute Proteinase K reaction, the sections were hybridized with spatial tags on the slides and reverse-transcribed in situ. The cDNAs were analyzed by RNA sequencing using DNBseq (MGI) with 300 million reads per sample. Raw FASTQ files and microscope slide images for each sample were processed with Space Ranger software (version 1.1, 10× Genomics) using the "spaceranger count" pipeline, involving STAR with the default parameters for aligning reads against the mouse reference genome mm10 "refdata-gex-mm10-2020-A." This pipeline uses Visium spatial barcodes to generate a feature spot matrix with unique molecular identifier counts. Clustering analysis was performed using Seurat (version 5.0.0)[52] and clusters were visualized using UMAP. Differentially expressed genes between genotypes were identified using an adjusted p-value < 0.05 and a fold change > 1.5. Metascape[33] and Enrichr[53] were used to analyze the GO terms and upstream transcription factors within each cluster, respectively. The Mouse Visium data were deposited to the GEO database (Accession No. GSE305995).

## scRNA-seq and data analysis

The 10x Genomics Chronium FRP protocol was followed for scRNA-seq analysis. On days 4 and 5 for WT, or day 4 evening and midnight for p38α floxed and uKO, uterine horns were excised, snap-frozen, and sent to Takara Bio Co.(Osaka, Japan). After fixing the cells with formaldehyde, a single-cell suspension was prepared using a GentleMACS (Miletenyi Biotec). The cells were used for RNA sequencing library preparation using the Chromium Next GEM Single Cell Fixed RNA Sample Preparation Kit, Chromium Fixed RNA Kit, Mouse Transcriptome, Chromium Mouse Transcriptome Probe Set v1.0.1, Chromium Next GEM Chip Q Single Cell Kit, Dual Index Kit TS Set A, and Chromium X (10x genomics, USA). Paired-end sequencing was performed on an Illumina next-generation sequencer (NovaSeq 6000; Illumina). Raw FASTQ files were processed using Cell Ranger software (10x Genomics, USA), and Seurat (*http://www.satijalab.org/seurat*) v5.0.0[52] was used to process read counts. Cell trajectory was determined using Monocle3[54]. CellChat was used for the cell-cell interaction assay. The mouse scRNA-seq data were deposited in the GEO database (Accession No. GSE296581 and GSE305994).

## Statistical analyses

Statistical analyses were performed using a two-tailed Student's *t*-test or one-way analysis of variance (ANOVA), followed by Bonferroni post-hoc tests, in GraphPad Prism10. Statistical significance was set at $P < 0.05$.

## Study approval

All animal experiments were approved by the Institutional Animal Experiment Committee of the University of Tokyo Graduate School of Medicine (approval numbers P20-076 and A2023M165).

## Data availability

The RNA-seq experimental data will be made publicly available upon publication (GSE305994 and GSE305995). This study did not involve the development of custom code or algorithms. All the software used in this study is publicly available and is cited in the main text and Methods sections.

## Acknowledgements

We thank Ms. Atsumi Miura for providing technical assistance. We are grateful to Francesco J. DeMayo (National Institute of Environmental Health Sciences) for providing Pgr-Cre mice, and to Kinya Otsuki (Osaka University) for providing *Mapk14*-floxed mice.

## Additional information

### Funding

This work was supported by the Japan Society for the Promotion of Science (JSPS) KAKENHI (grant nos. 23K08278, 23K27176, 24K22157, 24K21911, 25K02779, 25H01065), Japan Agency for Medical Research and Development (AMED) (grant no. JP25gn0110085, JP24gn0110069, JP25gk0210039, JP24lk0310083, JP25gn0110097, JP25gk0210042 and JP25gk0210045), Children and Families Agency (Grant Number JPMH23DB0101), Japan Science and Technology Agency (JST) Fusion Oriented Research for Disruptive Science and Technology (FOREST) (grant no. JPMJFR210H), Mochida Memorial Foundation for Medical and Pharmaceutical Research, Uehara Memorial Foundation, Inoue Foundation for Science, Astellas Foundation for Research on Metabolic Disorders, The Naito Foundation and the fund of joint research with NIPRO corporation.

### Author contributions

Conceptualization: S.A. and Y.H.; Funding acquisition: S.A. and Y.H.; Investigation:C.I., S.A., Y.F., X.H., R.S.H., D.H., T.H., M.M.; Data analysis: C.I., S.A.; Data interpretation: C.I., S.A., Y.H.; Project administration and supervision: Y.H.; Writing - original draft preparation: C.I., S.A.; Writing – review and editing: S.A.

### Funding


| Funder | Grant reference number | Author |
|---|---|---|
| MEXT \| Japan Society for the Promotion of Science (JSPS) | 23K08278 | Ryoko Shimizu-Hirota |
| MEXT \| Japan Society for the Promotion of Science (JSPS) | 23K27176 | Shizu Aikawa |
| MEXT \| Japan Society for the Promotion of Science (JSPS) | 24K22157 | Yasushi Hirota |
| MEXT \| Japan Society for the Promotion of Science (JSPS) | 24K21911 | Yasushi Hirota |
| MEXT \| Japan Society for the Promotion of Science (JSPS) | 25K02779 | Yasushi Hirota |
| MEXT \| Japan Society for the Promotion of Science (JSPS) | 25H01065 | Yasushi Hirota |
| Japan Agency for Medical Research and Development (AMED) | JP25gn0110085 | Yasushi Hirota |
| Japan Agency for Medical Research and Development (AMED) | JP24gn0110069 | Yasushi Hirota |
| Japan Agency for Medical Research and Development (AMED) | JP25gk0210039 | Yasushi Hirota |

| | | |
|---|---|---|
| Japan Agency for Medical Research and Development (AMED) | JP24lk0310083 | Yasushi Hirota |
| Japan Agency for Medical Research and Development (AMED) | JP25gn0110097 | Yasushi Hirota |
| Japan Agency for Medical Research and Development (AMED) | JP25gk0210042 | Yasushi Hirota |
| Japan Agency for Medical Research and Development (AMED) | JP25gk0210045 | Yasushi Hirota |
| Children and Families Agency | JPMH23DB0101 | Yasushi Hirota |
| MEXT \| Japan Science and Technology Agency (JST) | https://doi.org/10.52926/jpmjfr210h | Shizu Aikawa |
| Mochida Memorial Foundation for Medical and Pharmaceutical Research (公益財団法人 持田記念医学薬学振興財団) | | Shizu Aikawa |
| Uehara Memorial Foundation (UMF) | | Shizu Aikawa |
| Astellas Foundation for Research on Metabolic Disorders | | Shizu Aikawa |
| Inoue Foundation for Science | | Shizu Aikawa |
| Naito Foundation (内藤記念科学振興財団) | | Shizu Aikawa |
| Nipro (ニプロの) | | Yasushi Hirota |


## Author ORCID iDs

**Shizu Aikawa**: https://orcid.org/0000-0001-7407-4051
**Yasushi Hirota**: https://orcid.org/0000-0003-0241-9780

# Additional files

***Supplementary figures***

***Table S1***

***Table S2***

***Table S3***

***Table S4***

***Table S5***

***Table S6***

***Table S7***

***Table S8***

# References

1. **Anonymous** (2023) 1 in 6 people globally affected by infertility: WHO. *Saudi Med J* **44**:524-525 PubMed
2. **Dey SK,** et al. (2004) Molecular cues to implantation. *Endocrine reviews* **25**:341-373 https://doi.org/10.1210/er.2003-0020 | PubMed
3. **Fukui Y,** et al. (2019) Uterine receptivity, embryo attachment, and embryo invasion: Multistep processes in embryo implantation. *Reprod Med Biol* **18**:234-240 https://doi.org/10.1002/rmb2.12280 | PubMed
4. **Haraguchi H,** et al. (2014) MicroRNA-200a locally attenuates progesterone signaling in the cervix, preventing embryo implantation. *Mol Endocrinol* **28**:1108-1117 https://doi.org/10.1210/me.2014-1097 | PubMed

5. **Hirota Y** (2019) Progesterone governs endometrial proliferation-differentiation switching and blastocyst implantation. *Endocr J* **66**:199-206 https://doi.org/10.1507/endocrj.ej18-0431 | PubMed
6. **Gebril M,** et al. (2020) Uterine Epithelial Progesterone Receptor Governs Uterine Receptivity Through Epithelial Cell Differentiation. *Endocrinology* **161** https://doi.org/10.1210/endocr/bqaa195 | PubMed
7. **Zhang S,** et al. (2014) Uterine Rbpj is required for embryonic-uterine orientation and decidual remodeling via Notch pathway-independent and -dependent mechanisms. *Cell Res* **24**:925-942 https://doi.org/10.1038/cr.2014.82 | PubMed
8. **Egashira M,** Hirota Y (2013) Uterine receptivity and embryo-uterine interactions in embryo implantation: lessons from mice. *Reprod Med Biol* **12**:127-132 https://doi.org/10.1007/s12522-013-0153-1 | PubMed
9. **Fukui Y,** et al. (2021) Uterine Epithelial LIF Receptors Contribute to Implantation Chamber Formation in Blastocyst Attachment. *Endocrinology* **162** https://doi.org/10.1210/endocr/bqab169 | PubMed
10. **Yuan J,** Deng W, Cha J, Sun X, Borg JP, Dey SK (2018) Tridimensional visualization reveals direct communication between the embryo and glands critical for implantation. *Nature communications* **9** https://doi.org/10.1038/s41467-018-03092-4 | PubMed
11. **Aikawa S,** et al. (2024) Spatiotemporal functions of leukemia inhibitory factor in embryo attachment and implantation chamber formation. *Cell Death Discov* **10** https://doi.org/10.1038/s41420-024-02228-4 | PubMed
12. **Hiraoka T,** et al. (2020) Differential roles of uterine epithelial and stromal STAT3 coordinate uterine receptivity and embryo attachment. *Sci Rep* **10** https://doi.org/10.1038/s41598-020-72640-0 | PubMed
13. **Kobayashi R,** et al. (2014) The contribution of leukemia inhibitory factor (LIF) for embryo implantation differs among strains of mice. *Immunobiology* **219**:512-521 https://doi.org/10.1016/j.imbio.2014.03.011 | PubMed
14. **Sun X,** Bartos A, Whitsett JA, Dey SK (2013) Uterine deletion of Gp130 or Stat3 shows implantation failure with increased estrogenic responses. *Mol Endocrinol* **27**:1492-1501 https://doi.org/10.1210/me.2013-1086 | PubMed
15. **Akaeda S,** et al. (2021) Retinoblastoma protein promotes uterine epithelial cell cycle arrest and necroptosis for embryo invasion. *EMBO Rep* **22**:e50927 https://doi.org/10.15252/embr.202050927 | PubMed
16. **Fukui Y,** et al. (2023) The EZH2-PRC2-H3K27me3 axis governs the endometrial cell cycle and differentiation for blastocyst invasion. *Cell Death Dis* **14** https://doi.org/10.1038/s41419-023-05832-x | PubMed
17. **Coulthard LR,** White DE, Jones DL, McDermott MF, Burchill SA (2009) p38(MAPK): stress responses from molecular mechanisms to therapeutics. *Trends Mol Med* **15**:369-379 https://doi.org/10.1016/j.molmed.2009.06.005 | PubMed
18. **Morrison DK** (2012) MAP kinase pathways. *Cold Spring Harb Perspect Biol* **4** https://doi.org/10.1101/cshperspect.a011254 | PubMed
19. **Nishida K,** et al. (2004) p38alpha mitogen-activated protein kinase plays a critical role in cardiomyocyte survival but not in cardiac hypertrophic growth in response to pressure overload. *Mol Cell Biol* **24**:10611-10620 https://doi.org/10.1128/mcb.24.24.10611-10620.2004 | PubMed
20. **Zohn IE,** Li Y, Skolnik EY, Anderson KV, Han J, Niswander L (2006) p38 and a p38-interacting protein are critical for downregulation of E-cadherin during mouse gastrulation. *Cell* **125**:957-969 https://doi.org/10.1016/j.cell.2006.03.048 | PubMed
21. **Liu Y,** Martinez L, Ebine K, Abe MK (2008) Role for mitogen-activated protein kinase p38 alpha in lung epithelial branching morphogenesis. *Dev Biol* **314**:224-235 https://doi.org/10.1016/j.ydbio.2007.12.003 | PubMed
22. **Wen HC,** et al. (2011) p38α Signaling Induces Anoikis and Lumen Formation During Mammary Morphogenesis. *Sci Signal* **4**:ra34 https://doi.org/10.1126/scisignal.2001684 | PubMed

23. **Canovas B,** Nebreda AR (2021) Diversity and versatility of p38 kinase signalling in health and disease. *Nat Rev Mol Cell Biol* **22**:346-366 https://doi.org/10.1038/s41580-020-00322-w | PubMed

24. **Chen Y,** Ramakrishnan DP, Ren B (2013) Regulation of angiogenesis by phospholipid lysophosphatidic acid. *Front Biosci (Landmark Ed)* **18**:852-861 https://doi.org/10.2741/4148 | PubMed

25. **Tang Y,** et al. (2022) P38alpha MAPK is a gatekeeper of uterine progesterone responsiveness at peri-implantation via Ube3c-mediated PGR degradation. *Proc Natl Acad Sci U S A* **119**:e2206000119 https://doi.org/10.1073/pnas.2206000119 | PubMed

26. **Cha J,** Sun X, Dey SK (2012) Mechanisms of implantation: strategies for successful pregnancy. *Nat Med* **18**:1754-1767 https://doi.org/10.1038/nm.3012 | PubMed

27. **Cha J,** et al. (2014) Appropriate crypt formation in the uterus for embryo homing and implantation requires Wnt5a-ROR signaling. *Cell Rep* **8**:382-392 https://doi.org/10.1016/j.celrep.2014.06.027 | PubMed

28. **Arora R,** et al. (2016) Insights from imaging the implanting embryo and the uterine environment in three dimensions. *Development* **143**:4749-4754 https://doi.org/10.1242/dev.144386 | PubMed

29. **Ye X** (2020) Uterine Luminal Epithelium as the Transient Gateway for Embryo Implantation. *Trends Endocrinol Metab* **31**:165-180 https://doi.org/10.1016/j.tem.2019.11.008 | PubMed

30. **Psychoyos A** (1973) *Endocrine control of egg implantation* American Physiology Society.

31. **Xie Z,** et al. (2021) Gene Set Knowledge Discovery with Enrichr. *Curr Protoc* **1**:e90 https://doi.org/10.1002/cpz1.90 | PubMed

32. **Lau E,** Ronai ZA (2012) ATF2 - at the crossroad of nuclear and cytosolic functions. *J Cell Sci* **125**:2815-2824 https://doi.org/10.1242/jcs.095000 | PubMed

33. **Zhou Y,** et al. (2019) Metascape provides a biologist-oriented resource for the analysis of systems-level datasets. *Nature communications* **10**:1523 https://doi.org/10.1038/s41467-019-09234-6 | PubMed

34. **Stewart CL,** et al. (1992) Blastocyst implantation depends on maternal expression of leukaemia inhibitory factor. *Nature* **359**:76-79 https://doi.org/10.1038/359076a0 | PubMed

35. **Chen JR,** Cheng JG, Shatzer T, Sewell L, Hernandez L, Stewart CL (2000) Leukemia inhibitory factor can substitute for nidatory estrogen and is essential to inducing a receptive uterus for implantation but is not essential for subsequent embryogenesis. *Endocrinology* **141**:4365-4372 https://doi.org/10.1210/endo.141.12.7855 | PubMed

36. **Song H,** Lim H, Das SK, Paria BC, Dey SK (2000) Dysregulation of EGF family of growth factors and COX-2 in the uterus during the preattachment and attachment reactions of the blastocyst with the luminal epithelium correlates with implantation failure in LIF-deficient mice. *Mol Endocrinol* **14**:1147-1161 https://doi.org/10.1210/mend.14.8.0498 | PubMed

37. **Zhou C,** et al. (2021) Sequential activation of uterine epithelial IGF1R by stromal IGF1 and embryonic IGF2 directs normal uterine preparation for embryo implantation. *J Mol Cell Biol* **13**:646-661 https://doi.org/10.1093/jmcb/mjab034 | PubMed

38. **Matsumoto L,** et al. (2018) HIF2α in the uterine stroma permits embryo invasion and luminal epithelium detachment. *J Clin Invest* **128**:3186-3197 https://doi.org/10.1172/jci98931 | PubMed

39. **Bondarenko V,** et al. (2023) Embryo-uterine interaction coordinates mouse embryogenesis during implantation. *EMBO J* **42**:e113280 https://doi.org/10.15252/embj.2022113280 | PubMed

40. **Cha J,** Sun X, Dey SK (2012) Mechanisms of implantation: strategies for successful pregnancy. *Nat Med* **18**:1754-1767 https://doi.org/10.1038/nm.3012 | PubMed

41. **Ye X,** et al. (2005) LPA3-mediated lysophosphatidic acid signalling in embryo implantation and spacing. *Nature* **435**:104-108 https://doi.org/10.1038/nature03505 | PubMed

42. **Hama K,** et al. (2007) Embryo spacing and implantation timing are differentially regulated by LPA3-mediated lysophosphatidic acid signaling in mice. *Biol Reprod* **77**:954-959 https://doi.org/10.1095/biolreprod.107.060293 | PubMed

43. **Jinno M,** Ozaki T, Iwashita M, Nakamura Y, Kudo A, Hirano H (2001) Measurement of endometrial tissue blood flow: a novel way to assess uterine receptivity for implantation. *Fertil Steril* **76**:1168-1174 https://doi.org/10.1016/s0015-0282(01)02897-7 | PubMed

44. **Uchida H** (2024) Epithelial mesenchymal transition in human menstruation and implantation. *Endocr J* **71**:745-751 https://doi.org/10.1507/endocrj.ej24-0229 | PubMed

45. **Owusu-Akyaw A,** Krishnamoorthy K, Goldsmith LT, Morelli SS (2019) The role of mesenchymal-epithelial transition in endometrial function. *Hum Reprod Update* **25**:114-133 https://doi.org/10.1093/humupd/dmy035 | PubMed

46. **Whitby S,** Zhou W, Dimitriadis E (2020) Alterations in Epithelial Cell Polarity During Endometrial Receptivity: A Systematic Review. *Front Endocrinol (Lausanne)* **11** https://doi.org/10.3389/fendo.2020.596324 | PubMed

47. **Joseph S,** et al. (2025) MAPK14/p38α shapes the molecular landscape of endometrial cancer and promotes tumorigenic characteristics. *Cell Rep* **44** https://doi.org/10.1016/j.celrep.2024.115104 | PubMed

48. **Hiraoka T,** Osuga Y, Hirota Y (2023) Current perspectives on endometrial receptivity: A comprehensive overview of etiology and treatment. *J Obstet Gynaecol Res* **49**:2397-2409 https://doi.org/10.1111/jog.15759 | PubMed

49. **Soyal SM,** et al. (2005) Cre-mediated recombination in cell lineages that express the progesterone receptor. *Genesis* **41**:58-66 https://doi.org/10.1002/gene.20098 | PubMed

50. **Daikoku T,** et al. (2011) Conditional deletion of Msx homeobox genes in the uterus inhibits blastocyst implantation by altering uterine receptivity. *Dev Cell* **21**:1014-1025 https://doi.org/10.1016/j.devcel.2011.09.010 | PubMed

51. **Livak KJ,** Schmittgen TD (2001) Analysis of relative gene expression data using real-time quantitative PCR and the 2(-Delta Delta C(T)) Method. *Methods* **25**:402-408 https://doi.org/10.1006/meth.2001.1262 | PubMed

52. **Hao Y,** et al. (2024) Dictionary learning for integrative, multimodal and scalable single-cell analysis. *Nat Biotechnol* **42**:293-304 https://doi.org/10.1038/s41587-023-01767-y | PubMed

53. **Chen EY,** et al. (2013) Enrichr: interactive and collaborative HTML5 gene list enrichment analysis tool. *BMC Bioinformatics* **14** https://doi.org/10.1186/1471-2105-14-128 | PubMed

54. **Cao J,** et al. (2019) The single-cell transcriptional landscape of mammalian organogenesis. *Nature* **566**:496-502 https://doi.org/10.1038/s41586-019-0969-x | PubMed

**Aikawa S,** Ishizawa C, Hirota Y (2026) Single-cell gene expressions in p38α-deleted uteri before the embryo attachement. NCBI Gene Expression Omnibus. ID GSE305994 https://www.ncbi.nlm.nih.gov/geo/query/acc.cgi?acc=GSE305994

**Aikawa S,** Ishizawa C, Hirota Y (2026) Spatial gene expressions in p38α-deleted uteri after the embryo attachement. NCBI Gene Expression Omnibus. ID GSE305995 https://www.ncbi.nlm.nih.gov/geo/query/acc.cgi?acc=GSE305995

**Aikawa S,** He X, Hirota Y (2025) Mouse uterine gene expressions during decidual processes [scRNA-seq]. NCBI Gene Expression Omnibus. ID GSE296583 https://www.ncbi.nlm.nih.gov/geo/query/acc.cgi?acc=GSE296583

# Peer reviews

## Reviewer #1 (Public review):

Summary:

This manuscript asks how the uterine lumen is remodeled across the peri-implantation window and whether this remodeling is functionally linked to embryo attachment and subsequent pregnancy establishment. The authors combine whole-organ three-dimensional

imaging of optically cleared mouse uteri with single-cell and spatial transcriptomic profiling, conditional deletion of p38α at the uterine-wide versus epithelial-restricted level, and rescue experiments using progesterone and leukemia inhibitory factor. Based on these datasets, the authors propose that the luminal epithelium undergoes a previously underappreciated phase of organ-scale architectural reorganization before attachment, and that a p38α-dependent stress-responsive program coordinates epithelial remodeling together with epithelial-stromal communication required for implantation competence.

Strengths:

By moving beyond local attachment-site morphology to a horn-level representation of luminal topology, the work provides anatomical context that is difficult to reconstruct from conventional section-based approaches and should be broadly useful to the implantation community. The integration of organ-scale morphology with single-cell and spatial transcriptomic datasets, together with genetic perturbation and rescue experiments, adds breadth and increases the potential long-term utility of the dataset for investigators interested in uterine receptivity and embryo-uterine interactions.

Weaknesses:

(1) The whole-uterus analysis of luminal folds and creases requires stronger methodological support. Given the mechanical compliance of the uterine lumen, it is difficult to evaluate from the current description whether dissection, fixation, clearing, and/or mounting could influence the observed luminal topography. This issue is particularly important because several key conclusions depend on the spatial distribution of folds across the uterine horn. A fuller account of tissue handling and reconstruction, together with validation that the preparation preserves native morphology, would substantially strengthen confidence in the organ-scale conclusions.

(2) Several of the central morphological claims are supported primarily only by representative reconstructions. This includes the proposed flattening/creasing dynamics, alternating stretched and shrunken regions, persistence of abnormal folding in the mutant uterus, and the extent of structural rescue following progesterone supplementation. The authors could extract objective measures from the reconstructed luminal surface and provide more statistical analysis to demonstrate the reproducibility of the results.

(3) The manuscript appears to over-reach in concluding that luminal remodeling zones embryos before attachment from day 4 to 5. As presented, the data support a correlation between luminal architecture and embryo position, but do not discriminate between (i) luminal remodeling directing embryo positioning, (ii) embryos locally shaping the lumen, or (iii) parallel regulation of both. The evidence is based on observations of the uterus and the inside blastocysts at certain time points around implantation. Without the time-lapse analysis within the uterus, the dynamic interactions between embryos and the uterus couldn't be determined.

(4) The key conclusion of the manuscript is that uterine p38α regulates luminal epithelial remodeling required for embryo attachment, as shown in the title. Against this background, the finding that epithelial-restricted loss of p38α does not overtly impair fertility is notable, as it suggests that the major function of p38α may not be epithelial cell-autonomous but instead may arise through other uterine compartments that secondarily influence the epithelium. At present, however, this conclusion remains insufficiently supported: the epithelial-specific model is not characterized in sufficient depth during the peri-implantation period, and the transcriptomic evidence for altered epithelial-stromal communication does not by itself explain the phenotypic difference between uterine-wide and epithelial-specific deletion. If stromal p38α is proposed as the critical upstream regulator, more direct testing, such as stromal-specific deletion, would be needed.

https://doi.org/10.7554/eLife.110844.1.sa1

## Reviewer #2 (Public review):

Summary:

In this study, the authors aimed to characterize the architectural reorganization of the uterine luminal epithelium during the implantation period. Using 3D histological reconstruction, single-cell RNA sequencing, and spatial transcriptomics, the authors characterize luminal remodeling during the peri-implantation period and employ a mouse model to explore the role of p38α in regulating luminal flattening.

Strengths:

This study clearly described the changes in luminal architecture during implantation. Moreover, they also used integration of multiple advanced techniques, including 3D tissue reconstruction, single-cell transcriptomics, and spatial transcriptomics, which together provide a detailed description of the molecular characteristics of the uterine architecture during implantation.

Weaknesses:

The authors used PR-Cre to generate uterine p38α knockout mice. This Cre driver deletes p38α not only in epithelial cells but also in stromal compartments. Therefore, it remains unclear whether the observed phenotype arises from epithelial cells, stromal cells, or a combination of both. Previous studies have shown that p38α regulates epithelial polarity, cytoskeletal organization, and E-cadherin localization. However, the current study does not examine changes in cell adhesion or epithelial junction integrity. Previous studies have reported that uterine fluid absorption during implantation is closely associated with luminal closure and remodeling. It would be important to determine whether epithelial transport-related genes are altered in the mutant uterus. Could dysregulated fluid homeostasis contribute to the implantation defects observed in the p38α-deficient mice?

https://doi.org/10.7554/eLife.110844.1.sa0